

1                   **Magnetospheric control of ionospheric TEC**  
2                   **perturbations via whistler-mode and ULF waves**

3                   **Yangyang Shen<sup>1</sup>, Olga P. Verkhoglyadova<sup>2</sup>, Anton Artemyev<sup>1</sup>, Michael D.**  
4                   **Hartinger<sup>3,1</sup>, Vassilis Angelopoulos<sup>1</sup>, Xueling Shi<sup>4</sup>, Ying Zou<sup>5</sup>**

5                   <sup>1</sup>Department of Earth, Planetary, and Space Sciences, University of California, Los Angeles, CA, USA

6                   <sup>2</sup>Jet Propulsion Laboratory, California Institute of Technology, Pasadena, CA, USA

7                   <sup>3</sup>Space Science Institute, Center for Space Plasma Physics, Boulder, CO, USA

8                   <sup>4</sup>Department of Electrical and Computer Engineering, Virginia Tech, Blacksburg, VA, USA

9                   <sup>5</sup>Johns Hopkins University Applied Physics Laboratory, Laurel, MD, USA

10                   **Key Points:**

- 11                   • Space-ground conjugate observations point to magnetospheric whistler-mode waves  
12                   as the driver of ionospheric TEC perturbations (dTEC)
- 13                   • The amplitude spectra of dTEC and whistlers are consistent and the cross-correlation  
14                   between modeled and observed dTEC reaches 0.8
- 15                   • Whistler-mode wave amplitudes and dTEC are modulated by ULF waves, which  
16                   exhibit concurrent compressional and poloidal mode variations

---

Corresponding author: Yangyang Shen, [yshen@epss.ucla.edu](mailto:yshen@epss.ucla.edu)

**Abstract**

The weakly ionized plasma in the Earth's ionosphere is controlled by a complex interplay between solar and magnetospheric inputs from above, atmospheric processes from below, and plasma electrodynamics from within. This interaction results in ionosphere structuring and variability that pose major challenges for accurate ionosphere prediction for global navigation satellite system (GNSS) related applications and space weather research. The ionospheric structuring and variability are often probed using the total electron content (TEC) and its relative perturbations (dTEC). Among dTEC variations observed at high latitudes, a unique modulation pattern has been linked to magnetospheric ultra-low-frequency (ULF) waves, yet its underlying mechanisms remain unclear. Here using magnetically-conjugate observations from the THEMIS spacecraft and a ground-based GPS receiver at Fairbanks, Alaska, we provide direct evidence that these dTEC modulations are driven by magnetospheric electron precipitation induced by ULF-modulated whistler-mode waves. We observed peak-to-peak dTEC amplitudes reaching  $\sim 0.5$  TECU (1 TECU is equal to  $10^6$  electrons/m<sup>2</sup>) with modulations spanning scales of  $\sim 5$ –80 km. The cross-correlation between our modeled and observed dTEC reached  $\sim 0.8$  during the conjugacy period but decreased outside of it. The spectra of whistler-mode waves and dTEC also matched closely at ULF frequencies during the conjugacy period but diverged outside of it. Our findings elucidate the high-latitude dTEC generation from magnetospheric wave-induced precipitation, addressing a significant gap in current physics-based TEC modeling. These results thus improve ionospheric TEC prediction and enhance our understanding of magnetosphere-ionosphere coupling via ULF waves.

**Plain Language Summary**

Radio signals are refracted or diffracted as they traverse the ionosphere filled with free electrons. The ionosphere total electron content (TEC), which is the total number of electrons along the raypath from the satellite to a receiver, helps to correct refractive errors in the signal, while its relative perturbations (dTEC) can be used to probe diffractive fluctuations known as ionosphere scintillation. Refractive error degrades global navigation satellite system (GNSS) positioning service accuracy while scintillation leads to signal reception failures and disrupts navigation and communication. Thus, an accurate understanding and modeling of TEC and dTEC is vital for space weather monitoring and GNSS-related applications. This study analyzes fortuitous observations of ionospheric

dTEC from a ground-based GPS receiver and magnetospheric whistler-mode waves (a distinct type of very-low-frequency electromagnetic waves) from the THEMIS spacecraft, which were well-aligned both in time and space. We find a good cross-correlation ( $\sim 0.8$ ) between observed and modeled dTEC, driven by whistler-induced magnetospheric electron precipitation. These results point to whistler-mode waves as the driver of the observed dTEC. Both dTEC and whistler-mode wave amplitudes were modulated by ultra-low-frequency (ULF) waves. These findings enhance physics-based ionospheric TEC prediction and our understanding of magnetosphere-ionosphere coupling.

## 1 Introduction

The Earth’s ionosphere contains weakly ionized plasma in the atmosphere between approximately 80 km and 1000 km altitude. The state of ionospheric plasma is controlled by a complex interplay between solar and magnetospheric inputs from above, neutral atmospheric processes from below, and plasma electrodynamics from within. The resulting structuring and variability of ionospheric plasma have a major, adverse impact on the global navigation satellite system (GNSS) radio signals as they propagate through the ionosphere and experience varying degrees of refraction and diffraction (Morton et al., 2020). Refraction causes signal group delay and phase advance, leading to dominant errors in GNSS position, velocity, and time solutions, while diffraction causes stochastic intensity and phase fluctuations at the receiver, commonly known as ionospheric scintillation (Yeh & Liu, 1982; Rino, 2011). Scintillation leads to increased GNSS receiver measurement noise and errors and, in extreme cases, phase-tracking loss of lock or signal reception failures (Kintner et al., 2007). Thus, these ionospheric effects pose real threats to the reliability, continuity, and accuracy of GNSS operations and applications (Morton et al., 2020; Coster & Yizengaw, 2021). Understanding the causes for ionospheric structuring and variability is critical for forecasting their impacts on GNSS applications—a long-standing challenge for space weather research (Hey et al., 1946; Jakowski et al., 2011; Morton et al., 2020). The importance of this ionosphere forecasting has recently gained increased attention as the solar maximum unfolds and concerns over space weather events such as geomagnetic storms loom large (e.g., Kintner et al., 2007; Pulkkinen et al., 2017; Hapgood et al., 2022).

Ionospheric refraction is typically quantified by the total electron content (TEC), which is the total number of electrons within a unit cross section along the raypath ex-

81 tending from the receiver to the satellite. For dual-frequency GNSS or Global Position-  
82 ing System (GPS) receivers, the TEC is estimated from differential group delays and carrier-  
83 phase advances (Mannucci et al., 1998; Ciraolo et al., 2007; McCaffrey & Jayachandran,  
84 2017). Global TEC maps, constructed from networks of GNSS receivers on the ground  
85 and in orbit, can be used not only to correct ionospheric effects in GNSS-related appli-  
86 cations but also to monitor large- and meso-scale traveling ionospheric disturbances (TIDs),  
87 typically exceeding 100 km in horizontal wavelength (Hunsucker, 1982; Themens et al.,  
88 2022; S.-R. Zhang et al., 2022). TIDs may result from internal ionospheric dynamics or  
89 from atmospheric effects from below linked to natural hazards, such as tsunamis, earth-  
90 quakes, explosions, and volcanic eruptions (Komjathy et al., 2016; Astafyeva, 2019). High-  
91 resolution TEC from individual receivers and its relative perturbations (dTEC) and rate  
92 of changes (ROTI) are often used for detecting small-scale ionospheric irregularities and  
93 scintillation events (Pi et al., 1997; Cherniak et al., 2014; McCaffrey & Jayachandran,  
94 2019; Makarevich et al., 2021; Nishimura et al., 2023).

95 One of the main challenges in ionospheric TEC modeling and space weather pre-  
96 diction is the complex structuring and variability of ionosphere plasma. Rapid (<a few  
97 minutes) and small-scale (<~100 km) TEC perturbations are observed at both low and  
98 high latitudes but generated by distinct mechanisms and drivers (Pi et al., 1997; Basu  
99 et al., 2002; Kintner et al., 2007; Spogli et al., 2009; Moen et al., 2013; Pilipenko et al.,  
100 2014; Jin et al., 2015; Prikryl et al., 2015; Watson, Jayachandran, Singer, et al., 2016;  
101 Fæhn Follestad et al., 2020). Near equatorial latitudes, these small-scale TEC pertur-  
102 bations result from plasma bubbles or density depletions formed around post-sunset, pri-  
103 marily driven by the Rayleigh-Taylor instability associated with lower atmosphere-ionosphere  
104 coupling processes (C.-S. Huang & Kelley, 1996; Kelley, 2009; Xiong et al., 2010; Aa et  
105 al., 2020; Jin et al., 2020). At high latitudes, TEC perturbations are associated with plasma  
106 irregularities in the auroral, cusp, and polar cap regions, spanning a few meters to hun-  
107 dreds of kilometers in spatial scale (e.g., Basu et al., 1990; Moen et al., 2013; Spicher et  
108 al., 2017). These irregularities are primarily driven by solar-magnetosphere-ionosphere  
109 coupling, which involves a complex interplay and synergy among solar extreme-ultraviolet  
110 (EUV) radiation, plasma  $\mathbf{E} \times \mathbf{B}$  drifts, charged-particle precipitation into the atmosphere,  
111 magnetic field-aligned currents, and various ionospheric plasma instabilities (Kelley, 2009;  
112 Moen et al., 2013; Spicher et al., 2015; Fæhn Follestad et al., 2020).

113 Among dTEC variations observed near the auroral latitudes, a unique modulation  
114 pattern has been linked to magnetospheric ultra-low-frequency (ULF) waves (Davies &  
115 Hartmann, 1976; Okuzawa & Davies, 1981; Skone, 2009; Pilipenko et al., 2014; Watson  
116 et al., 2015; Watson, Jayachandran, Singer, et al., 2016; Zhai et al., 2021). These ULF  
117 waves feature broadband or quasi-monochromatic geomagnetic pulsations with periods  
118 from about 0.2 to 600 s (Jacobs et al., 1964) and are considered to be crucial for energy  
119 and plasma transport throughout the solar-magnetosphere-ionosphere-thermosphere sys-  
120 tem (e.g., Southwood & Kivelson, 1981; M. K. Hudson et al., 2000, 2008; Hartinger et  
121 al., 2015, 2022; Zong et al., 2017). Skone (2009) noted that average power of ground-based  
122 ULF waves and TEC perturbations exhibited similar temporal variations in the Pc3 band  
123 ( $\sim 22$ – $100$  mHz). Pilipenko et al. (2014) observed a high coherence ( $\sim 0.9$ ) between TEC  
124 perturbations and global Pc5 pulsations in a few mHz during a geomagnetic storm. Watson,  
125 Jayachandran, Singer, et al. (2016) also reported a high coherence and common power  
126 between TEC perturbations and ULF radial magnetic field variations in the Pc4 band  
127 (6.7–22 mHz). Fully understanding ULF-induced ionospheric TEC perturbations not only  
128 enhances the ionosphere forecasting during space weather events but also elucidates the  
129 critical pathways of geospace energy coupling and dissipation via ULF waves.

130 To date, despite numerous proposals for direct TEC modulation mechanisms by  
131 ULF waves (Pilipenko et al., 2014), no mechanism has yet been conclusively established.  
132 Recently, Wang et al. (2020) have reported a storm-time event where duskside ionospheric  
133 density was modulated by ULF waves in the Pc5 range. Density inversion from radar  
134 data suggests that Pc5 pulsations modulated precipitating electrons over an energy range  
135 of  $\sim 1$ – $500$  keV and an altitude range of  $\sim 80$ – $200$  km. Higher-energy precipitating elec-  
136 trons deposit their energy and induce impact ionization at lower altitudes, whereas lower-  
137 energy electrons do so at higher altitudes. The authors postulated that the precipita-  
138 tion and density perturbations are likely due to electron pitch-angle scattered into the  
139 loss cone by ULF-modulated very-low-frequency (VLF) whistler-mode waves.

140 This postulation is supported by extensive observations and models that demon-  
141 strate that ULF waves often coexist with and modulate whistler-mode waves (Coroniti  
142 & Kennel, 1970; W. Li, Thorne, et al., 2011; W. Li, Bortnik, Thorne, Nishimura, et al.,  
143 2011; Watt et al., 2011; Jaynes et al., 2015; Xia et al., 2016, 2020; X.-J. Zhang et al., 2019;  
144 X. J. Zhang et al., 2020; X. Shi et al., 2022; L. Li et al., 2022, 2023). The modulation  
145 of the whistler-mode wave growth is potentially attributed to compression-induced am-

146 bient thermal or resonant hot electron density variations (W. Li, Bortnik, Thorne, Nishimura,  
147 et al., 2011; Xia et al., 2016, 2020; X.-J. Zhang et al., 2019; X. J. Zhang et al., 2020),  
148 resonant electron anisotropy variations (W. Li, Thorne, et al., 2011; Watt et al., 2011),  
149 and nonlinear resonant effects from periodic magnetic field configuration variations (L. Li  
150 et al., 2022, 2023). The periodic excitation of whistler-mode waves at ULF wave frequen-  
151 cies leads to periodic electron precipitation, which drives pulsating auroras (e.g., Miyoshi  
152 et al., 2010; Nishimura et al., 2010; Jaynes et al., 2015) and potentially explains many  
153 previously reported TEC modulations at ULF frequencies (Pilipenko et al., 2014; Wat-  
154 son, Jayachandran, Singer, et al., 2016; Zhai et al., 2021).

155 However, it is challenging to establish a direct link between magnetospheric drivers  
156 and ionospheric TEC perturbations during ULF modulation events due to several com-  
157 plicating factors: (1) the path-integrated nature of TEC perturbations, which strongly  
158 depend on the satellite-to-receiver raypath elevation (e.g., Jakowski et al., 1996; Kom-  
159 jathy, 1997), (2) inherent phase shifts due to coexisting propagation and modulation ef-  
160 fects (Watson et al., 2015), particularly when conjugate observations are misaligned or  
161 not synchronized, and (3) the dynamic and turbulent nature of the auroral ionosphere  
162 (Kelley, 2009). Direct evidence linking TEC perturbations to magnetospheric drivers is  
163 yet to be identified.

164 In this study, fortuitously conjugate observations from the THEMIS spacecraft and  
165 the GPS receiver at Fairbanks, Alaska (FAIR) allow us to identify the driver of GPS TEC  
166 perturbations as magnetospheric electron precipitation induced by ULF-modulated whistler-  
167 mode waves. Figure 1 illustrates the physical picture emerging from these magnetically-  
168 conjugate magnetospheric and ionospheric observations of ULF waves, modulated whistler-  
169 mode waves, electron precipitation, and TEC perturbations.

170 In what follows, Section 2 describes datasets and models employed to estimate whistler-  
171 driven precipitation and resulting TEC perturbations. Section 3 presents a detailed anal-  
172 ysis and cross-correlation between observed and modeled TEC perturbations. Section  
173 4 discusses the geophysical implications and applications of our results, which are fol-  
174 lowed by the main conclusions.

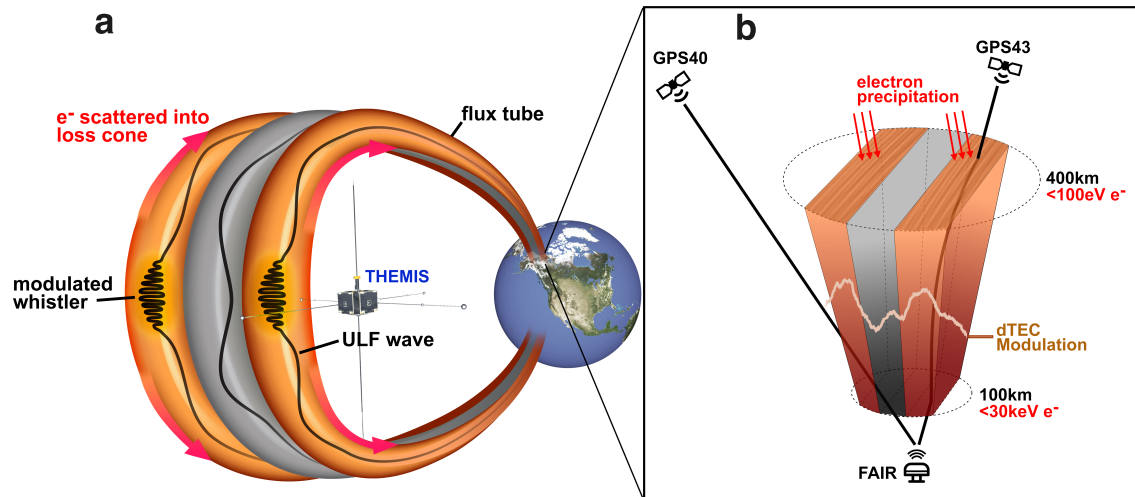


**Figure 1.** Schematic diagram showing coordinated observations from THEMIS and FAIR of (a) modulation of very-low-frequency (VLF) whistler-mode waves near the magnetic equator by ultra-low-frequency (ULF) waves, electron pitch-angle scattering into the loss cone, and precipitation into the ionosphere (red arrows) induced by modulated whistler-mode waves; and (b) the modulated electron precipitation with energies of  $\sim 0.1\text{--}30$  keV deposits their energies at altitudes between  $\sim 100\text{--}400$  km and induces modulated impact ionization and TEC perturbations (dTEC) having amplitudes as large as  $\sim 0.5$  TECU and spanning scales of  $\sim 5\text{--}80$  km. This dTEC modulation was captured by the signal from GPS43, which has a high elevation, but was overlooked by the signal from GPS40, which has a relatively lower elevation.

## 2 Data and Methodology

We derive 1-s vertical TEC (VTEC) measurements from phase and pseudorange data collected by the GPS receiver at Fairbanks, Alaska (FAIR) during 15:06–16:36 UT on July 3, 2013, processed at Jet Propulsion Laboratory using the GipsyX and Global Ionospheric Mapping (GIM) software (Komjathy et al., 2005; Bertiger et al., 2020). Phase-based TEC measurements are leveled using pseudorange delays for each phase-connected data collection. We focus on links between FAIR and GPS satellites with pseudo random noise (PRN) numbers 40, 43, and 60, referred to as GPS40, GPS43, and GPS60, whose ionospheric pierce points (IPP) at 450 km altitude are within 300 km proximity to FAIR, or IPPs at 150 km are within 100 km proximity to FAIR. The obtained TEC is expressed in TEC units (TECU), i.e.,  $10^{16}$  electrons/m<sup>2</sup>. The slant TEC is converted to VTEC using the standard mapping function (e.g., Mannucci et al., 1998). Measurements with elevation angles less than 30° are not considered here. The VTEC data are then detrended to get TEC perturbations (dTEC) using a fourth-order Butterworth low-pass filter. We focus on dTEC with wave periods smaller than 25 min.

We use the following datasets from THEMIS-E (Angelopoulos, 2008): electron energy and pitch-angle distributions measured by the Electrostatic Analyzers (ESA) instrument in the energy range of several eV up to 30 keV (McFadden et al., 2008), DC vector magnetic field at spin resolution ( $\sim 3$  s) measured by the Fluxgate Magnetometers (FGM) (Auster et al., 2008), electric and magnetic field wave spectra within 1 Hz–4 kHz, measured every  $\sim 8$  s by the Digital Fields Board (DFB), the Electric Field Instrument (EFI), and the search coil magnetometer (SCM) (Le Contel et al., 2008; Bonnell et al., 2008; Cully, Ergun, et al., 2008). Background electron densities are inferred from spacecraft potentials (Bonnell et al., 2008; Nishimura et al., 2013). We also use ground-based magnetometer measurements every 1 s from the College (CMO) site operated by the United States Geological Survey Geomagnetism Program and from the Fort Yukon (FYKN) site operated by the Geophysical Institute at the University of Alaska.

THEMIS observations of electron distributions and wave spectra allow us to calculate the precipitating flux of electrons scattered into the loss cone by whistler-mode waves using quasilinear diffusion theory (Kennel & Engelmann, 1966; Lyons, 1974). For whistler-mode wave normals  $\theta < 45^\circ$ , we use a validated analytical formula of bounce-averaged electron diffusion coefficients from Artemyev et al. (2013). For small pitch an-



207 gle  $\alpha_{eq}$  approaching the loss cone  $\alpha_{LC}$ , the first-order cyclotron resonance provides the  
 208 main contribution to the bounce-averaged diffusion rate:

$$\langle D_{\alpha_{eq}\alpha_{eq}} \rangle \simeq \frac{\pi B_w^2 \Omega_{ceq} \omega_m}{4\gamma B_{eq}^2 \Delta\omega (p\epsilon_{meq})^{13/9} T(\alpha_{LC}) \cos^2_{\alpha_{LC}}} \times \frac{\Delta\lambda_{R,N} (1 + 3 \sin^2 \lambda_R)^{7/12} (1 - \bar{\omega})}{|\gamma\bar{\omega} - 2\gamma\bar{\omega}^2 + 1| |1 - \gamma\bar{\omega}|^{4/9}}, \quad (1)$$

209 with  $B_w$  indicating the wave amplitude,  $\omega_m$  the mean wave frequency,  $\Delta\omega$  the frequency  
 210 width,  $\bar{\omega} = \omega_m/\Omega_{ce}$  the normalized frequency,  $\Omega_{ce}$  and  $\Omega_{ceq}$  the local and equatorial  
 211 electron cyclotron frequency,  $\gamma$  the relativistic factor,  $p$  the electron momentum,  $\epsilon_{meq} =$   
 212  $\Omega_{pe}/\Omega_{ceq} \sqrt{\omega_m/\Omega_{ceq}}$  where  $\Omega_{pe}$  is the plasma frequency,  $T(\alpha_{eq})$  the bounce period,  $\lambda_R$   
 213 the latitude of resonance, and  $\Delta\lambda_{R,N}$  the latitudinal range of resonance (see details in  
 214 Artemyev et al. (2013)). The precipitating differential energy flux within the loss cone  
 215 can be estimated as  $x(E)J(E, \alpha_{LC})$ , where

$$x(E) = 2 \int_0^1 I_0(Z_0\tau) \tau d\tau / I_0(Z_0), \quad (2)$$

216 being the index of loss cone filling,  $J(E, \alpha_{LC})$  is the electron differential energy flux near  
 217 the loss cone,  $I_0$  is the modified Bessel function with an argument  $Z_0 \simeq \alpha_{LC} / \sqrt{\langle D_{\alpha_{eq}\alpha_{eq}} \rangle \cdot \tau_{loss}}$   
 218 (Kennel & Petschek, 1966), and  $\tau_{loss}$  is assumed to be half of the bounce period.

219 With an energy distribution of precipitating electrons within 0.1–30 keV, we es-  
 220 timate the impact ionization rate altitude profile using the parameterization model de-  
 221 veloped by Fang et al. (2010), covering isotropic electron precipitation from 100 eV up  
 222 to 1 MeV. This model, derived through fits to first-principle model results, allows effi-  
 223 cient ionization computation for arbitrary energy spectra. Atmospheric density and scale  
 224 height data were obtained from the NRLMSISE-00 model (Picone et al., 2002). We model  
 225 TEC perturbations resulting from whistler-induced electron precipitation by integrat-  
 226 ing ionization rates over altitude and time, adopting an 8-s integration period to align  
 227 with the temporal resolution of THEMIS wave spectra data. Although our analysis does  
 228 not concern equilibrium densities and omits recombination and convective effects, this  
 229 neglect has little impact because we focus on relative TEC perturbations due to short-  
 230 time precipitation. It takes nearly 60 s for the background ionosphere to relax to an equi-  
 231 librium density solution for 10-keV precipitation and longer for lower energies (e.g., Kaep-  
 232 pler et al., 2022). Our estimated dTEC also closely match observed dTEC values, un-  
 233 derscoring the effectiveness of our modeling approach despite its approximation.

### 3 Results

On July 3, 2013, from 15:06 to 16:36 UT, the THEMIS-E spacecraft flew westward over the FAIR GPS receiver station, coming within  $\sim 20$  km relative to FAIR when mapped to 450 km altitude. This optimally timed and positioned space-ground conjunction offers a unique opportunity to link between magnetospheric and ionospheric processes along the field line. The event occurred at  $L \sim 7$ , outside the plasmopause of  $L_{pp} \sim 5.4$  (based on THEMIS-E densities near 17:00 UT), near the magnetic local time ( $MLT$ ) of 4.5 hr, and during a geomagnetic quiet time with  $Kp \sim 1$  and  $AE \sim 200$  nT. Figure 2a illustrates the trajectories of THEMIS-E and the ionosphere pierce points (IPPs) of GPS40, GPS43, and GPS60 near FAIR, mapped to 450 km altitude. The footprints of THEMIS-E are field-line traced using the Tsyganenko T96 model (Tsyganenko, 1995) but the GPS satellites are mapped using line of sight. Of these GPS satellites, the GPS43 IPPs, moving eastward, were nearest to both the FAIR and THEMIS-E footprints, exhibiting close longitudinal alignment. A notable conjugacy, marked by the bright red segment from 15:37 to 16:11 UT, occurred when the footprints of THEMIS-E and GPS43 IPPs were within  $\sim 100$  km to each other and FAIR (Figure 2j). In Supporting Information, we also present the configuration when the satellites and their IPPs are mapped to an altitude of 150 km. This adjustment does not significantly alter the geometry of our conjunction event, but it does slightly reduce the scale of the satellite footpaths near FAIR.

Figures 2b–2d present THEMIS observations of whistler-mode waves. The observed wave frequencies were in the whistler lower band, spanning  $\sim 0.2$ – $0.5\Omega_{ce}$ , with a mean frequency  $\omega_m \sim 0.35\Omega_{ce}$ , and  $\Delta\omega \sim 0.15\Omega_{ce}$ , where the electron cyclotron frequency  $f_{ce} \sim \Omega_{ce}/2\pi \sim 2.15$  kHz. Figure 2d shows that whistler-mode wave amplitudes  $B_w$  range from several pT to over 100 pT, measured at 8-s cadence (black curve) and smoothed with 2-min moving averages (red curve). Short-term oscillations in  $B_w$  on the order of tens of seconds were observed atop more gradual variations of several minutes. We mainly use smoothed or average  $B_w$  to estimate electron precipitation in the following. Absent direct waveform data on whistler-mode wave normals for our event, we infer, based on the measured  $E/cB$  spectra ( $E/cB \ll 1$ , see Supporting Information) and statistical night-side equatorial plasma sheet observations (W. Li, Bortnik, Thorne, & Angelopoulos, 2011; Agapitov et al., 2013; Meredith et al., 2021), the presence of quasi-parallel whistlers with an assumed Gaussian wave normal width of  $\Delta\theta \sim 30^\circ$  confined within  $\pm 30^\circ$  in latitude.

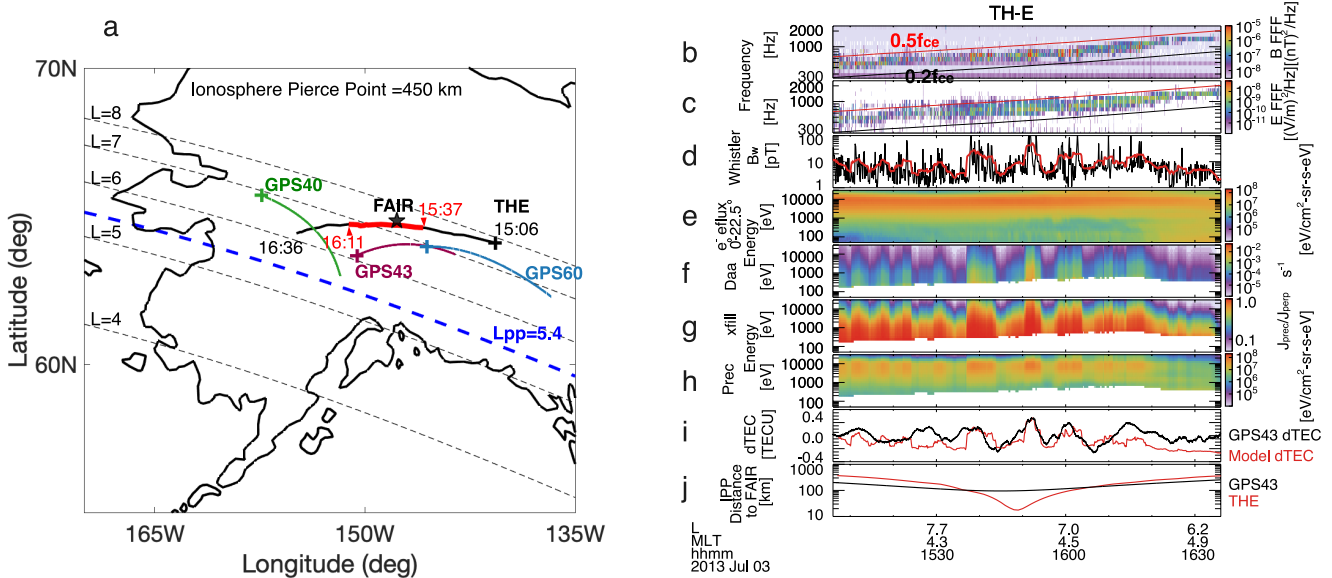


**Figure 2.** (a) Configuration of THEMIS-E (black curve), GPS40, GPS43, and GPS60 satellites (green, purple, and blue curves), and the FAIR receiver (black star) in geographic coordinates, with THEMIS and GPS mapped onto 450 km altitude using T96 field tracing (THEMIS) or line of sight (GPS). The plus symbol indicates the start of the footpath. (b–e) THEMIS-E magnetic field spectrogram, electric field spectrogram, whistler-mode wave amplitudes, and field-aligned ( $0^\circ$ – $22.5^\circ$ ) electron energy spectrogram. (f) Bounce-averaged electron diffusion rates. (g) Index of loss cone filling. (h) Whistler-driven precipitating electron energy spectrogram. (i) Comparison of whistler-driven model dTEC (red curve) and GPS43-observed dTEC (black curve). (j) Great-circle distances between THEMIS-E footpath (red curve) and GPS43 raypath (black curve) at IPP of 450 km relative to the FAIR station.

266 Figures 2e-2h display the measured plasma sheet field-aligned ( $\alpha \sim [0^\circ, 22.5^\circ]$ ) elec-  
 267 trons from 50 eV up to 25 keV, calculated diffusion rates  $\langle D_{\alpha_{eq}\alpha_{eq}} \rangle$ , estimated loss cone  
 268 filling  $x(E)$ , and precipitating electron energy fluxes. Although  $\langle D_{\alpha_{eq}\alpha_{eq}} \rangle$  and  $x(E)$  in-  
 269 crease at lower energies, the precipitating energy fluxes peak between 1-10 keV, exhibit-  
 270 ing similar modulations as seen in the smoothed whistler-mode wave amplitude  $B_w$ . Elec-  
 271 tron precipitation fluxes below  $\sim 200$  eV are absent due to an energy threshold for elec-  
 272 tron cyclotron resonance interaction, with the lower limit primarily determined by the  
 273 ratio  $\Omega_{pe}/\Omega_{ce}$  ( $\sim 3$  in our case).

274 Figure 2i compares modeled (red) and directly measured dTEC (black) from the  
 275 GPS43 signal, revealing a nearly one-to-one phase correlation from 15:37 to 16:11 UT.  
 276 This period of close correlation coincides with the conjunction of THEMIS-E, GPS43,  
 277 and FAIR, where their relative distances were within  $\sim 100$  km (Figure 2j). Outside this  
 278 conjugacy period and further away from the FAIR station, the correlation decreases. Ob-  
 279 served peak-to-peak amplitudes of dTEC reached  $\sim 0.5$  TECU. Note that this particu-  
 280 lar event occurred during quiet conditions; other events during storms may have much  
 281 larger TEC modulation amplitudes (e.g., Watson et al., 2015), though more challeng-  
 282 ing to have such reliable conjunction, especially given uncertainties in magnetic field map-  
 283 ping during storms (e.g., C.-L. Huang et al., 2008).

284 Figure 3 underscores the critical role of observation geometry and timing in detect-  
 285 ing phase correlations between modeled and measured dTEC across three GPS satellites.  
 286 Despite all three satellites having raypath elevation angles  $> 40^\circ$ —reducing the likelihood  
 287 of multi-path effects (e.g., Kintner et al., 2007)—only the GPS43 elevation reached  $80^\circ$   
 288 above the FAIR station zenith (Figure 3a). During the conjugacy period, the IPPs of  
 289 GPS40 and GPS60 were distanced from FAIR by more than 200 km, while GPS43’s IPPs  
 290 remained within 100 km, coming within 20 km at its closest point (Figure 3b). Figures 3c  
 291 and 3d reveal that the modeled dTEC (red curve) aligns poorly with GPS40 and GPS60  
 292 dTEC (blue and magenta curves), but a significant cross-correlation ( $\sim 0.8$ ) emerges with  
 293 GPS43 dTEC (black) during the conjugacy period. Before and after the conjunction, TEC  
 294 phase shifts reduce the cross-correlation to -0.15 and 0.68, respectively. Given the near-  
 295 parallel longitudinal alignment of GPS43 IPPs and THEMIS-E footprints (Figure 2a),  
 296 the measured dTEC (black) potentially reflects both temporal and spatial/longitudinal  
 297 modulations. These findings suggest that to reliably identify the electron precipitation

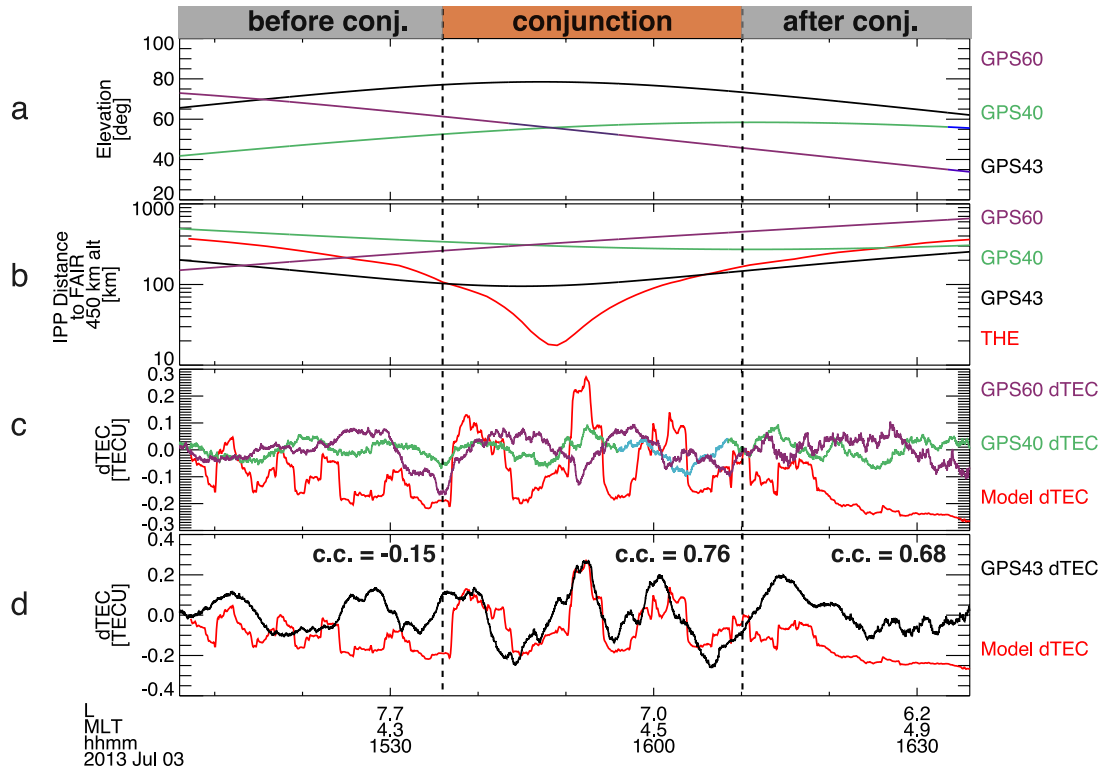


**Figure 3.** (a) Raypath elevation angles of GPS40 (green curve), GPS43 (black curve), and GPS60 (magenta curve). (b) Distances between THEMIS-E footpath and GPS satellite IPPs relative to FAIR, displayed in the same format as Figure 1j. (c) Comparison between whistler-driven model dTEC and observed dTEC from GPS40 and GPS60, which were not in good conjunction with THEMIS or FAIR. (d) Comparison between whistler-driven model dTEC and GPS43-observed dTEC. The cross-correlation coefficients are -0.15, 0.76, and 0.68 during intervals before, during, and after conjunction, respectively.

298 responsible for TEC perturbations requires precise spacecraft spatial alignment, opti-  
 299 mal timing, and high raypath elevations.

300 The modulation of TEC perturbations, electron precipitation, and whistler-mode  
 301 wave amplitudes was linked to ULF wave activities in the Pc3-5 band (1.7 mHz to 100  
 302 mHz). Figure 4a display the magnetic field perturbations measured by THEMIS-E in  
 303 the mean field-aligned (MFA) coordinates, in which the parallel direction ( $\parallel$ , the com-  
 304 pressional component) is determined by 15-minute sliding averages of the magnetic field,  
 305 the azimuthal direction ( $\phi$ , the toroidal component) is along the cross product of  $z$  and  
 306 the spacecraft geocentric position vector, and the radial direction ( $r$ , the poloidal com-  
 307 ponent) completes the triad. Magnetic perturbations are obtained by subtracting the  
 308 15-minute mean field. During the conjunction, THEMIS-E detected both compressional  
 309 Pc5 waves (red curve) and poloidal Pc3-4 waves (blue curve). Figure 4b indicates that  
 310 peaks in whistler-mode wave amplitudes approximately align with troughs of compres-  
 311 sional ULF waves, with fine-scale whistler amplitudes primarily modulated by poloidal  
 312 Pc3-4 waves (See Supporting Information). Strong Pc5 ULF waves were also recorded  
 313 in the  $H$ -component magnetic field perturbations from magnetometers located at CMO  
 314 and FYKN (Figures 4g–4h), displaying a similar pattern but with greater amplitudes  
 315 at FYKN, located slightly north of FAIR. The discrepancy between ground- and space-  
 316 measured Pc5 waves potentially results from the localized nature of THEMIS-E obser-  
 317 vations (X. Shi et al., 2022) and the screening/modification effects of ULF waves travers-  
 318 ing the ionosphere (Hughes & Southwood, 1976; Lysak, 1991; Lessard & Knudsen, 2001;  
 319 X. Shi et al., 2018). These observations imply that the ionospheric TEC perturbations  
 320 were linked to ULF-modulated whistler-mode waves and the associated electron precip-  
 321 itation (e.g., Coroniti & Kennel, 1970; W. Li, Thorne, et al., 2011; Xia et al., 2016; X. J. Zhang  
 322 et al., 2020; L. Li et al., 2023).

323 Figures 4b–4c compare small-scale/high-frequency fluctuations of whistler-mode  
 324 wave amplitudes  $B_w$  and dTEC, which was bandpass-filtered within the frequency range  
 325 of 5–200 mHz. The small-scale dTEC fluctuations exhibit similar wave periods to  $B_w$   
 326 fluctuations, evidently intensifying during the conjugacy period, yet lacking a clear phase  
 327 correlation seen with larger scale perturbations in Figure 3d. Assumed purely spatial,  
 328 small-scale dTEC variations have wavelengths of  $\sim 15$ –30 km at IPPs of 450 km altitude  
 329 (or  $\sim 5$ –10 km at IPPs of 150 km altitude), compared with the larger-scale dTEC wave-  
 330 lengths of  $\sim 80$  km (or  $\sim 25$  km at IPPs of 150 km altitude). When mapped to the mag-

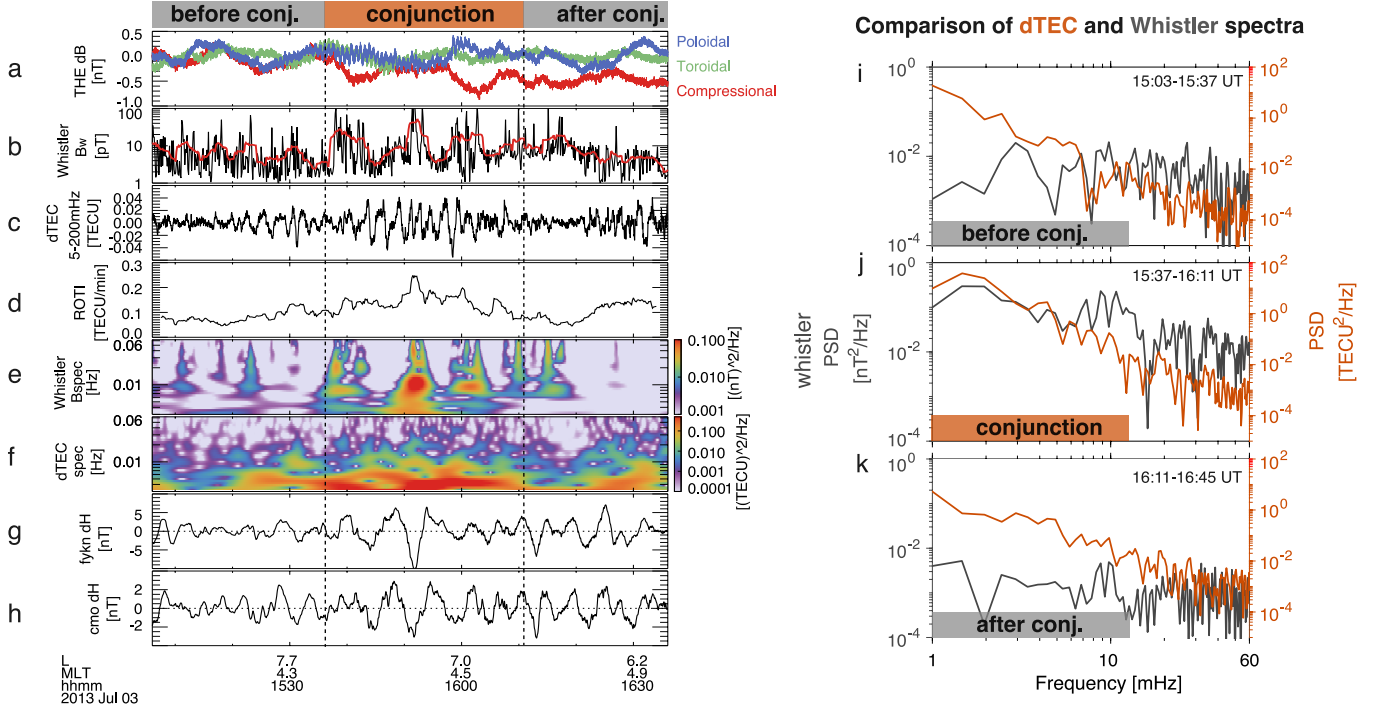


**Figure 4.** (a) THEMIS-E magnetic field perturbations in the mean-field-aligned (MFA) coordinates, exhibiting primarily compressional- (red) and poloidal-mode (blue) variations. (b) THEMIS-E whistler-mode wave amplitudes. The measured amplitudes are shown in black and smoothed in red. (c) dTEC bandpass filtered within 5–200 mHz. (d) The rate of dTEC changes (*ROTI*) from 200-s sliding window ensemble averaging. (e) Wavelet spectrogram of whistler-mode waves. (f) Wavelet spectrogram of GPS43 dTEC. (g) Ground-based magnetic field *H* component perturbations in 1.7–100 mHz from the Fort Yukon station (FYKN). (h) Ground-based magnetic *H* component perturbations in 1.7–100 mHz from the College station (CMO). (i–k) Comparisons of dTEC (orange curves) and whistler-mode wave amplitude fluctuation spectra (gray curves) in 1–60 mHz measured before (i), during (j), and after (k) the conjugacy period.

331 netosphere, these small-scale dTEC modulations correspond to a magnetospheric source  
 332 region of  $\sim 100\text{--}700$  km, while large-scale dTEC modulations suggest a source region of  
 333  $\sim 500\text{--}2000$  km. These scales align with prior observations of the transverse scale sizes  
 334 of chorus elements and their source regions (Santolík et al., 2003; Agapitov et al., 2017,  
 335 2018), and with the azimuthal wavelengths of high-m poloidal ULF waves (Yeoman et  
 336 al., 2012; X. Shi et al., 2018; Zong et al., 2017). Figure 4d shows the rate of TEC index  
 337 (*ROTI*), i.e., the standard deviation of the rate of TEC (*ROT*) (Pi et al., 1997), where  
 338  $ROT = (dTEC(t+\tau) - dTEC(t))/\tau$  with  $\tau = 10$  s,  $ROTI = \sqrt{\langle ROT^2 \rangle - \langle ROT \rangle^2}$  us-  
 339 ing 200-s sliding averages. Significant increases in *ROTI* were observed within the re-  
 340 gion of whistler-driven TEC perturbations. However, in our case the GPS signal fluc-  
 341 tuations were predominantly refractive, as negligible fluctuations were detected at fre-  
 342 quencies above 0.1 Hz (McCaffrey & Jayachandran, 2017, 2019; Nishimura et al., 2023).

343 Figures 4e–4f compare the wavelet spectrograms of whistler-mode wave  $B_w$  and dTEC,  
 344 displaying concurrent increases in wave power for both in the frequency range of  $\sim 3$  mHz  
 345 up to tens of mHz. Figures 4i–4k present a more detailed amplitude spectra compari-  
 346 son before, during, and after conjunction. Notably, only during the conjunction, whistler-  
 347 mode wave amplitudes and dTEC share similar power spectral density (PSD) distribu-  
 348 tions in the 1– $\sim 30$  mHz range. The peaks in whistler spectra were slightly and consis-  
 349 tently larger than those in dTEC spectra within 3–20 mHz by factors of 1.05–1.2, align-  
 350 ing with expected Doppler shift effects on ionospheric TEC measurements. The Doppler  
 351 shift results from relative motion of GPS raypath (or IPPs with velocities of  $\sim 160$  m/s  
 352 in our case) and propagating TEC structures (typically with velocities of several hun-  
 353 dred m/s) (Watson, Jayachandran, & MacDougall, 2016):  $f_{cor} = f_{obs} \left(1 + \frac{\mathbf{v}_{ipp} \cdot \mathbf{v}_{struct}}{|\mathbf{v}_{struct}|^2}\right)$ ,  
 354 where  $f_{cor}$  is the frequency corrected for relative motion. Watson, Jayachandran, and  
 355 MacDougall (2016) found that 89% of their statistical events required a correction fac-  
 356 tor of 1.2 or less for the Doppler shift, consistent with our observations. The agreement  
 357 between dTEC and whistler amplitude spectra supports that the observed dTEC resulted  
 358 from electron precipitation induced by whistler-mode waves.

359 Figure 5 indicates that the electron precipitation, induced by ULF-modulated whistler-  
 360 mode waves, can cause significant increases in ionospheric ionization rate or column den-  
 361 sity, leading to TEC perturbations of  $\sim 0.36$  TECU with a moderate whistler amplitude  
 362 of  $B_w \sim 25$  pT. Given that large-amplitude whistler-mode waves exceeding several hun-  
 363 dred pT frequently occur in the inner magnetosphere (Cattell et al., 2008; Cully, Bon-



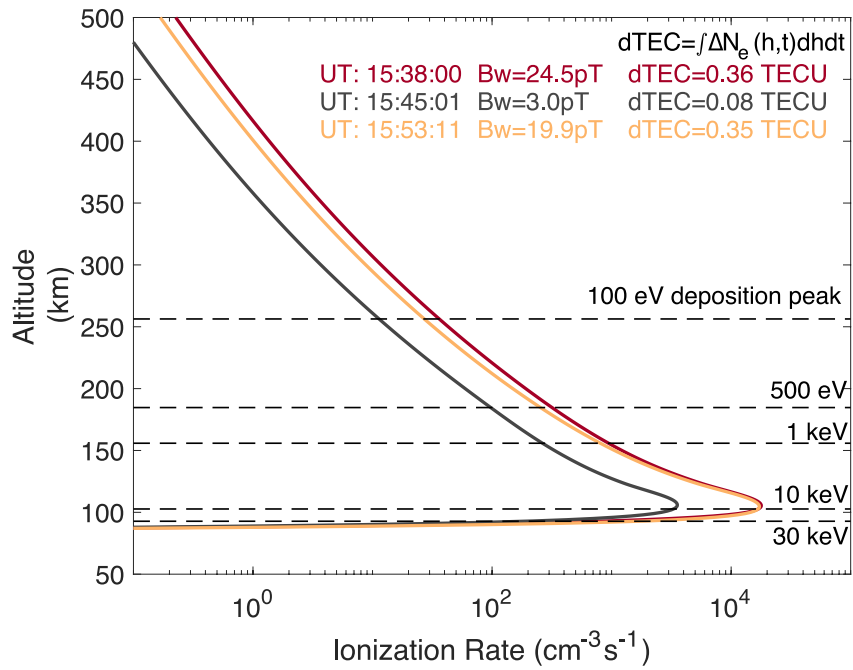


**Figure 5.** Ionization rate altitude profiles calculated at three time stamps of 15:38:00, 15:45:01, and 15:53:11 UT, corresponding to whistler-mode wave amplitudes of  $B_w = 24.5$  pT (red curve), 3.0 pT (gray curve), and 19.9 pT (orange curve). The dTEC were calculated by integrating ionization rates over altitude and time (8s). The dashed lines mark the peak deposition altitudes of 100 eV, 500 eV, 1 keV, 10 keV, and 30 keV precipitating monoenergetic electrons.

364 nell, & Ergun, 2008; Agapitov et al., 2014; Hartley et al., 2016; R. Shi et al., 2019), we  
365 anticipate even larger TEC perturbations from such whistler activities. We defer a sta-  
366 tistical study including storm time events and the potential connection with scintilla-  
367 tion (e.g., McCaffrey & Jayachandran, 2019; Nishimura et al., 2023) for the future. In  
368 addition, the primary energy range of precipitation spans from  $\sim 100$  eV to  $\sim 30$  keV, con-  
369 tributing to density variations between  $\sim 90$ – $\sim 400$  km (Fang et al., 2010; Katoh et al.,  
370 2023; Berland et al., 2023).

## 371 4 Discussion

372 Various mechanisms have been proposed that link ULF waves to TEC perturba-  
373 tions and ionospheric disturbances in general (Pilipenko et al., 2014). Although TEC per-  
374 turbations might arise from direct ULF wave effects through convective and divergent  
375 flows, MHD Alfvén-mode waves do not directly alter plasma density. Furthermore, mode-  
376 converted compressional waves, if present due to Hall currents, are evanescent in the iono-  
377 sphere (Lessard & Knudsen, 2001), resulting in negligible TEC perturbations (Pilipenko  
378 et al., 2014), especially when the ground-based magnetic perturbations were only sev-  
379 eral nT in our case (Figure 4g). A non-linear “feedback instability” mechanism may mod-  
380 ify ULF wave dynamics, causing field-aligned current striations and significant bottom-  
381 side ionospheric density cavities and gradients (Lysak, 1991; Streltsov & Lotko, 2008).  
382 Furthermore, ULF-induced plasma flows may result in gradient drift instabilities and den-  
383 sity striations and irregularities with scale sizes less than  $\sim 10$  km, in the presence of pre-  
384 existing larger-scale density gradients (Keskinen & Ossakow, 1983; Basu et al., 1990; Gondarenko  
385 & Guzdar, 2004; Kelley, 2009; Spicher et al., 2015; Nishimura et al., 2021). Addition-  
386 ally, electron precipitation and Joule heating are important factors to consider in the au-  
387 roral region (e.g., Deng & Ridley, 2007; Sheng et al., 2020; Meng et al., 2022).

388 Detecting one-to-one phase correlation between ground-based ULF waves and TEC  
389 perturbations may be challenging, largely due to ionospheric screening effects on ULF  
390 waves (Hughes & Southwood, 1976), with only a few exceptions noted during storm times  
391 (Pilipenko et al., 2014; Wang et al., 2020). However, this correlation has been frequently  
392 observed with spacecraft measurements of ULF waves (Watson et al., 2015; Watson, Jay-  
393 achandran, Singer, et al., 2016; Zhai et al., 2021), indicating that magnetospheric pro-  
394 cesses may play an important role in driving ionospheric TEC perturbations. Our find-  
395 ings support that magnetospheric whistler-mode waves, modulated by ULF waves in the

396 Pc3–5 band, are responsible for these periodic TEC perturbations through associated  
397 electron precipitation.

398 These results enhance our understanding of TEC modulation by ULF waves, a topic  
399 widely discussed in the literature (Skone, 2009; Pilipenko et al., 2014; Watson et al., 2015;  
400 Watson, Jayachandran, Singer, et al., 2016; Wang et al., 2020; Zhai et al., 2021), and fa-  
401 cilitates the integration of effects of magnetospheric whistler-mode waves into auroral  
402 TEC models. Statistical modeling of whistler-mode and ULF waves has been improv-  
403 ing for several decades (e.g., Tsurutani & Smith, 1974; McPherron, 1972; Southwood &  
404 Hughes, 1983; Takahashi & Anderson, 1992; M. Hudson et al., 2004; Claudepierre et al.,  
405 2010; W. Li, Bortnik, Thorne, & Angelopoulos, 2011; Agapitov et al., 2013; Artemyev  
406 et al., 2016; Tyler et al., 2019; Zong et al., 2017; Ma et al., 2020; X. J. Zhang et al., 2020;  
407 Sandhu et al., 2021; Hartinger et al., 2015, 2022, 2023). Leveraging these wave effects  
408 and the associated electron precipitation can enhance physics-based modeling of iono-  
409 spheric TEC by providing better specifications of high-latitude drivers (Schunk et al.,  
410 2004; Ridley et al., 2006; Zettergren & Snively, 2015; Meng et al., 2016, 2020; Sheng et  
411 al., 2020; Verkhoglyadova et al., 2020; Huba & Drob, 2017). This wave-driven precip-  
412 itation provides the dominant energy input to the ionosphere among all types of auro-  
413 ral precipitation (e.g., Newell et al., 2009), thus critically contributing to TEC pertur-  
414 bations at high latitudes. As such, incorporating these magnetospheric phenomena is vi-  
415 tal for improving the accuracy of ionospheric TEC models. This incorporation poten-  
416 tially benefits both GNSS-based applications and magnetosphere and ionosphere cou-  
417 pling science.

## 418 5 Conclusions

419 We present a detailed case study of ionospheric TEC perturbations (dTEC), us-  
420 ing magnetically-conjugate observations from the THEMIS spacecraft and the GPS re-  
421 ceiver at Fairbanks, Alaska (FAIR). This conjunction setup allows us to identify the mag-  
422 netospheric driver of the observed dTEC. Our key findings are summarized below:

- 423 • Combining in-situ wave and electron observations and quasilinear theory, we have  
424 modeled the electron precipitation induced by observed whistler-mode waves and  
425 deduced ionospheric dTEC based on impact ionization prediction. The cross-correlation

- 426 between our modeled and observed dTEC reached  $\sim 0.8$  during the conjugacy pe-  
427 riod of  $\sim 30$  min but decreased outside of it.
- 428 • Observed peak-to-peak dTEC amplitudes reached  $\sim 0.5$  TECU, exhibiting mod-  
429 ulations spanning scales of  $\sim 5$ – $80$  km. Within the modulated dTEC, enhancements  
430 in the rate of TEC index (ROTI) were measured to be  $\sim 0.2$  TECU/min.
  - 431 • The whistler-mode waves and dTEC modulations were linked to ULF waves in the  
432 Pc3-5 band, featuring concurrent compressional and poloidal mode fluctuations.  
433 The amplitude spectra of whistler-mode waves and dTEC also agreed from 1 mHz  
434 to tens of mHz during the conjugacy period but diverged outside of it.

435 Thus, our results provide direct evidence that ULF-modulated whistler-mode waves  
436 in the magnetosphere drive electron precipitation leading to ionospheric dTEC modu-  
437 lations. Our observations also indicate that to reliably identify the electron precipita-  
438 tion responsible for TEC perturbations requires precise spacecraft spatial alignment, op-  
439 timal timing, and high raypath elevations. Our findings elucidate the high-latitude dTEC  
440 generation from magnetospheric wave-induced precipitation, which has not been adequately  
441 addressed in physics-based TEC models. Consequently, these results improve ionospheric  
442 TEC prediction and enhance our understanding of magnetosphere-ionosphere coupling  
443 via ULF waves.

#### 444 **Acknowledgments**

445 This work has been supported by NASA projects 80NSSC23K0413, 80NSSC24K0138,  
446 and 80NSSC23K1038. Portions of the research were carried out at the Jet Propulsion  
447 Laboratory, California Institute of Technology, under a contract with NASA. O.P.V., M.D.H.,  
448 and X.S. were supported by NASA project 80NSSC21K1683. X.S. is supported by NASA  
449 award 80NSSC21K1677. O.P.V. would like to thank A.W. Moore (JPL) for data process-  
450 ing discussions. We are indebted to Emmanuel Masongsong for help with the schematic  
451 figure.

#### 452 **Open Research**

453 THEMIS data are available at [http://themis.ssl.berkeley.edu/data/themis/  
454 the/12/](http://themis.ssl.berkeley.edu/data/themis/the/12/). GPS RINEX data are publicly available from the NASA CDDIS archive of space  
455 geodesy data ([https://cddis.nasa.gov/Data\\_and\\_Derived\\_Products/GNSS/high-rate](https://cddis.nasa.gov/Data_and_Derived_Products/GNSS/high-rate)

456 \_data.html). TEC data derived for this study is available at [https://doi.org/10.48577/](https://doi.org/10.48577/jpl.LGI5JS)  
 457 [jpl.LGI5JS](https://doi.org/10.48577/jpl.LGI5JS) (Verkhoglyadova, 2024). The access and processing of THEMIS and ground-  
 458 based magnetic field data from CMO and FYKN was done using SPEDAS V4.1, see Angelopoulos  
 459 et al. (2019). The original CMO data are provided by the USGS Geomagnetism Program  
 460 (<http://geomag.usgs.gov>) but can be accessed through [http://themis.ssl.berkeley](http://themis.ssl.berkeley.edu/data/themis/thg/12/mag/cmo/2013/)  
 461 [.edu/data/themis/thg/12/mag/cmo/2013/](http://themis.ssl.berkeley.edu/data/themis/thg/12/mag/cmo/2013/). FYKN data are part of the Geophysical  
 462 Institute Magnetometer Array operated by the Geophysical Institute, University of Alaska  
 463 (<https://www.gi.alaska.edu/monitors/magnetometer/archive>).

## 464 References

- 465 Aa, E., Zou, S., Eastes, R., Karan, D. K., Zhang, S.-R., Erickson, P. J., & Coster,  
 466 A. J. (2020, January). Coordinated Ground-Based and Space-Based Observa-  
 467 tions of Equatorial Plasma Bubbles. *Journal of Geophysical Research (Space*  
 468 *Physics)*, *125*(1), e27569. doi: 10.1029/2019JA027569
- 469 Agapitov, O. V., Artemyev, A., Krasnoselskikh, V., Khotyaintsev, Y. V., Moure-  
 470 nas, D., Breuillard, H., ... Rolland, G. (2013, June). Statistics of whistler  
 471 mode waves in the outer radiation belt: Cluster STAFF-SA measurements. *J.*  
 472 *Geophys. Res.*, *118*, 3407-3420. doi: 10.1002/jgra.50312
- 473 Agapitov, O. V., Artemyev, A., Mourenas, D., Krasnoselskikh, V., Bonnell, J., Le  
 474 Contel, O., ... Angelopoulos, V. (2014). The quasi-electrostatic mode of  
 475 chorus waves and electron nonlinear acceleration. *J. Geophys. Res.*, *119*,  
 476 1606–1626. doi: 10.1002/2013JA019223
- 477 Agapitov, O. V., Blum, L. W., Mozer, F. S., Bonnell, J. W., & Wygant, J. (2017,  
 478 March). Chorus whistler wave source scales as determined from multipoint  
 479 Van Allen Probe measurements. *Geophys. Res. Lett.*, *44*, 2634-2642. doi:  
 480 10.1002/2017GL072701
- 481 Agapitov, O. V., Mourenas, D., Artemyev, A., Mozer, F. S., Bonnell, J. W., An-  
 482 gelopoulos, V., ... Krasnoselskikh, V. (2018, October). Spatial Extent and  
 483 Temporal Correlation of Chorus and Hiss: Statistical Results From Multipoint  
 484 THEMIS Observations. *Journal of Geophysical Research (Space Physics)*,  
 485 *123*(10), 8317-8330. doi: 10.1029/2018JA025725
- 486 Angelopoulos, V. (2008, December). The THEMIS Mission. *Space Sci. Rev.*, *141*, 5-  
 487 34. doi: 10.1007/s11214-008-9336-1

- 488 Angelopoulos, V., Cruce, P., Drozdov, A., Grimes, E. W., Hatzigeorgiu, N., King,  
 489 D. A., ... Schroeder, P. (2019, January). The Space Physics Environ-  
 490 ment Data Analysis System (SPEDAS). *Space Sci. Rev.*, *215*, 9. doi:  
 491 10.1007/s11214-018-0576-4
- 492 Artemyev, A. V., Agapitov, O., Mourenas, D., Krasnoselskikh, V., Shastun, V., &  
 493 Mozer, F. (2016, April). Oblique Whistler-Mode Waves in the Earth's Inner  
 494 Magnetosphere: Energy Distribution, Origins, and Role in Radiation Belt Dy-  
 495 namics. *Space Sci. Rev.*, *200*(1-4), 261-355. doi: 10.1007/s11214-016-0252-5
- 496 Artemyev, A. V., Mourenas, D., Agapitov, O. V., & Krasnoselskikh, V. V. (2013,  
 497 April). Parametric validations of analytical lifetime estimates for radiation belt  
 498 electron diffusion by whistler waves. *Annales Geophysicae*, *31*, 599-624. doi:  
 499 10.5194/angeo-31-599-2013
- 500 Astafyeva, E. (2019, December). Ionospheric Detection of Natural Hazards. *Reviews*  
 501 *of Geophysics*, *57*(4), 1265-1288. doi: 10.1029/2019RG000668
- 502 Auster, H. U., Glassmeier, K. H., Magnes, W., Aydogar, O., Baumjohann,  
 503 W., Constantinescu, D., ... Wiedemann, M. (2008, December). The  
 504 THEMIS Fluxgate Magnetometer. *Space Sci. Rev.*, *141*, 235-264. doi:  
 505 10.1007/s11214-008-9365-9
- 506 Basu, S., Groves, K. M., Basu, S., & Sultan, P. J. (2002, November). Specification  
 507 and forecasting of scintillations in communication/navigation links: current  
 508 status and future plans. *Journal of Atmospheric and Solar-Terrestrial Physics*,  
 509 *64*(16), 1745-1754. doi: 10.1016/S1364-6826(02)00124-4
- 510 Basu, S., MacKenzie, E., Basu, S., Coley, W. R., Sharber, J. R., & Hoegy, W. R.  
 511 (1990, June). Plasma structuring by the gradient drift instability at high lati-  
 512 tudes and comparison with velocity shear driven processes. *J. Geophys. Res.*,  
 513 *95*(A6), 7799-7818. doi: 10.1029/JA095iA06p07799
- 514 Berland, G. D., Marshall, R. A., Capannolo, L., McCarthy, M. P., & Zheng, L.  
 515 (2023, November). Kinetic Modeling of Radiation Belt Electrons With Geant4  
 516 to Study Energetic Particle Precipitation in Earth's Atmosphere. *Earth and*  
 517 *Space Science*, *10*(11), e2023EA002987. doi: 10.1029/2023EA002987
- 518 Bertiger, W., Bar-Sever, Y., Dorsey, A., Haines, B., Harvey, N., Hemberger, D., ...  
 519 Willis, P. (2020, August). GipsyX/RTGx, a new tool set for space geodetic  
 520 operations and research. *Advances in Space Research*, *66*(3), 469-489. doi:

- 521 10.1016/j.asr.2020.04.015
- 522 Bonnell, J. W., Mozer, F. S., Delory, G. T., Hull, A. J., Ergun, R. E., Cully, C. M.,  
523 ... Harvey, P. R. (2008, December). The Electric Field Instrument (EFI) for  
524 THEMIS. *Space Sci. Rev.*, *141*, 303-341. doi: 10.1007/s11214-008-9469-2
- 525 Cattell, C., Wygant, J. R., Goetz, K., Kersten, K., Kellogg, P. J., von Rosenvinge,  
526 T., ... Russell, C. T. (2008, January). Discovery of very large amplitude  
527 whistler-mode waves in Earth's radiation belts. *Geophys. Res. Lett.*, *35*, 1105.  
528 doi: 10.1029/2007GL032009
- 529 Cherniak, I., Krankowski, A., & Zakharenkova, I. (2014, August). Observation of  
530 the ionospheric irregularities over the Northern Hemisphere: Methodology and  
531 service. *Radio Science*, *49*(8), 653-662. doi: 10.1002/2014RS005433
- 532 Ciruolo, L., Azpilicueta, F., Brunini, C., Meza, A., & Radicella, S. M. (2007). Cali-  
533 bration errors on experimental slant total electron content (TEC) determined  
534 with GPS. *Journal of Geodesy*, *81*, 111-120.
- 535 Claudepierre, S. G., Hudson, M. K., Lotko, W., Lyon, J. G., & Denton, R. E. (2010,  
536 November). Solar wind driving of magnetospheric ULF waves: Field line res-  
537 onances driven by dynamic pressure fluctuations. *Journal of Geophysical Re-*  
538 *search (Space Physics)*, *115*(A11), A11202. doi: 10.1029/2010JA015399
- 539 Coroniti, F. V., & Kennel, C. F. (1970, March). Electron precipitation pulsations.  
540 *J. Geophys. Res.*, *75*(7), 1279-1289. doi: 10.1029/JA075i007p01279
- 541 Coster, A. J., & Yizengaw, E. (2021). Gnss/gps degradation from space weather.  
542 In *Space weather effects and applications* (p. 165-181). American Geophysical  
543 Union (AGU). doi: <https://doi.org/10.1002/9781119815570.ch8>
- 544 Cully, C. M., Bonnell, J. W., & Ergun, R. E. (2008, June). THEMIS observations  
545 of long-lived regions of large-amplitude whistler waves in the inner magneto-  
546 sphere. *Geophys. Res. Lett.*, *35*, 17. doi: 10.1029/2008GL033643
- 547 Cully, C. M., Ergun, R. E., Stevens, K., Nammari, A., & Westfall, J. (2008, Decem-  
548 ber). The THEMIS Digital Fields Board. *Space Sci. Rev.*, *141*, 343-355. doi:  
549 10.1007/s11214-008-9417-1
- 550 Davies, K., & Hartmann, G. K. (1976, July). Short-period fluctuations in total  
551 columnar electron content. *J. Geophys. Res.*, *81*(19), 3431. doi: 10.1029/  
552 JA081i019p03431
- 553 Deng, Y., & Ridley, A. J. (2007, September). Possible reasons for underestimat-

- 554 ing Joule heating in global models: E field variability, spatial resolution, and  
 555 vertical velocity. *Journal of Geophysical Research (Space Physics)*, *112*(A9),  
 556 A09308. doi: 10.1029/2006JA012006
- 557 Fæhn Follestad, A., Herlingshaw, K., Ghadjari, H., Knudsen, D. J., McWilliams,  
 558 K. A., Moen, J. I., . . . Oksavik, K. (2020, June). Dayside Field-Aligned  
 559 Current Impacts on Ionospheric Irregularities. *Geophys. Res. Lett.*, *47*(11),  
 560 e86722. doi: 10.1029/2019GL086722
- 561 Fang, X., Randall, C. E., Lummerzheim, D., Wang, W., Lu, G., Solomon, S. C.,  
 562 & Frahm, R. A. (2010, November). Parameterization of monoenergetic  
 563 electron impact ionization. *Geophys. Res. Lett.*, *37*(22), L22106. doi:  
 564 10.1029/2010GL045406
- 565 Gondarenko, N. A., & Guzdar, P. N. (2004, September). Plasma patch structuring  
 566 by the nonlinear evolution of the gradient drift instability in the high-latitude  
 567 ionosphere. *Journal of Geophysical Research (Space Physics)*, *109*(A9),  
 568 A09301. doi: 10.1029/2004JA010504
- 569 Hapgood, M., Liu, H., & Lugaz, N. (2022, March). SpaceX—Sailing Close  
 570 to the Space Weather? *Space Weather*, *20*(3), e2022SW003074. doi:  
 571 10.1029/2022SW00307410.1002/essoar.10510636.1
- 572 Hartinger, M. D., Elsdén, T., Archer, M. O., Takahashi, K., Wright, A. N., Arte-  
 573 myev, A., . . . Angelopoulos, V. (2023, December). Properties of Magneto-  
 574 hydrodynamic Normal Modes in the Earth’s Magnetosphere. *Journal*  
 575 *of Geophysical Research (Space Physics)*, *128*(12), e2023JA031987. doi:  
 576 10.1029/2023JA031987
- 577 Hartinger, M. D., Moldwin, M. B., Zou, S., Bonnell, J. W., & Angelopoulos, V.  
 578 (2015, January). ULF wave electromagnetic energy flux into the ionosphere:  
 579 Joule heating implications. *Journal of Geophysical Research (Space Physics)*,  
 580 *120*(1), 494-510. doi: 10.1002/2014JA020129
- 581 Hartinger, M. D., Takahashi, K., Drozdov, A. Y., Shi, X., Usanova, M. E., & Kress,  
 582 B. (2022, April). ULF Wave Modeling, Effects, and Applications: Accom-  
 583 plishments, Recent Advances, and Future. *Frontiers in Astronomy and Space*  
 584 *Sciences*, *9*, 867394. doi: 10.3389/fspas.2022.867394
- 585 Hartley, D. P., Kletzing, C. A., Kurth, W. S., Bounds, S. R., Averkamp, T. F.,  
 586 Hospodarsky, G. B., . . . Watt, C. E. J. (2016, May). Using the cold plasma



- 587 dispersion relation and whistler mode waves to quantify the antenna sheath  
 588 impedance of the Van Allen Probes EFW instrument. *Journal of Geophysical*  
 589 *Research (Space Physics)*, *121*(5), 4590-4606. doi: 10.1002/2016JA022501
- 590 Hey, J. S., Parsons, S. J., & Phillips, J. W. (1946, August). Fluctuations in Cos-  
 591 mic Radiation at Radio-Frequencies. *Nature*, *158*(4007), 234. doi: 10.1038/  
 592 158234a0
- 593 Huang, C.-L., Spence, H. E., Singer, H. J., & Tsyganenko, N. A. (2008, April).  
 594 A quantitative assessment of empirical magnetic field models at geosyn-  
 595 chronous orbit during magnetic storms. *Journal of Geophysical Research*  
 596 *(Space Physics)*, *113*(A4), A04208. doi: 10.1029/2007JA012623
- 597 Huang, C.-S., & Kelley, M. C. (1996, January). Nonlinear evolution of equatorial  
 598 spread F. 2. Gravity wave seeding of Rayleigh-Taylor instability. *J. Geophys.*  
 599 *Res.*, *101*(A1), 293-302. doi: 10.1029/95JA02210
- 600 Huba, J. D., & Drob, D. (2017, June). SAMI3 prediction of the impact of the 21  
 601 August 2017 total solar eclipse on the ionosphere/plasmasphere system. *Geo-*  
 602 *phys. Res. Lett.*, *44*(12), 5928-5935. doi: 10.1002/2017GL073549
- 603 Hudson, M., Denton, R., Lessard, M., Miftakhova, E., & Anderson, R. (2004, Jan-  
 604 uary). A study of Pc-5 ULF oscillations. *Annales Geophysicae*, *22*(1), 289-302.  
 605 doi: 10.5194/angeo-22-289-2004
- 606 Hudson, M. K., Elkington, S. R., Lyon, J. G., & Goodrich, C. C. (2000, Jan-  
 607 uary). Increase in Relativistic Electron Flux in the Inner Magnetosphere:  
 608 ULF Wave Mode Structure. *Advances in Space Research*, *25*(12), 2327-2337.  
 609 doi: 10.1016/S0273-1177(99)00518-9
- 610 Hudson, M. K., Kress, B. T., Mueller, H.-R., Zastrow, J. A., & Bernard Blake, J.  
 611 (2008, March). Relationship of the Van Allen radiation belts to solar wind  
 612 drivers. *Journal of Atmospheric and Solar-Terrestrial Physics*, *70*, 708-729.  
 613 doi: 10.1016/j.jastp.2007.11.003
- 614 Hughes, W. J., & Southwood, D. J. (1976, July). The screening of micropulsation  
 615 signals by the atmosphere and ionosphere. *J. Geophys. Res.*, *81*(19), 3234.  
 616 doi: 10.1029/JA081i019p03234
- 617 Hunsucker, R. D. (1982, May). Atmospheric Gravity Waves Generated in the High-  
 618 Latitude Ionosphere: A Review (Paper 1R1822). *Reviews of Geophysics and*  
 619 *Space Physics*, *20*, 293. doi: 10.1029/RG020i002p00293

- 620 Jacobs, J. A., Kato, Y., Matsushita, S., & Troitskaya, V. A. (1964, January). Classi-  
 621 fication of Geomagnetic Micropulsations. *J. Geophys. Res.*, *69*, 180-181. doi:  
 622 10.1029/JZ069i001p00180
- 623 Jakowski, N., Mayer, C., Hoque, M., & Wilken, V. (2011). Total electron content  
 624 models and their use in ionosphere monitoring. *Radio Science*, *46*(06), 1–11.
- 625 Jakowski, N., Sardon, E., Engler, E., Jungstand, A., & Klähn, D. (1996, De-  
 626 cember). Relationships between GPS-signal propagation errors and  
 627 EISCAT observations. *Annales Geophysicae*, *14*(12), 1429-1436. doi:  
 628 10.1007/s00585-996-1429-0
- 629 Jaynes, A. N., Lessard, M. R., Takahashi, K., Ali, A. F., Malaspina, D. M., Michell,  
 630 R. G., ... Wygant, J. R. (2015, October). Correlated Pc4-5 ULF waves,  
 631 whistler-mode chorus, and pulsating aurora observed by the Van Allen  
 632 Probes and ground-based systems. *J. Geophys. Res.*, *120*, 8749-8761. doi:  
 633 10.1002/2015JA021380
- 634 Jin, Y., Moen, J. I., & Miloch, W. J. (2015). On the collocation of the cusp au-  
 635 rora and the GPS phase scintillation: A statistical study. *Journal of Geophysi-  
 636 cal Research: Space Physics*, *120*(10), 9176–9191.
- 637 Jin, Y., Xiong, C., Clausen, L., Spicher, A., Kotova, D., Brask, S., ... Miloch, W.  
 638 (2020, July). Ionospheric Plasma Irregularities Based on In Situ Measurements  
 639 From the Swarm Satellites. *Journal of Geophysical Research (Space Physics)*,  
 640 *125*(7), e28103. doi: 10.1029/2020JA028103
- 641 Kaeppeler, S. R., Marshall, R., Sanchez, E. R., Juarez Madera, D. H., Troyer, R., &  
 642 Jaynes, A. N. (2022, December). pyGPI5: A python D- and E-region chem-  
 643 istry and ionization model. *Frontiers in Astronomy and Space Sciences*, *9*,  
 644 338. doi: 10.3389/fspas.2022.1028042
- 645 Katoh, Y., Rosendahl, P. S., Ogawa, Y., Hiraki, Y., & Tadokoro, H. (2023, Decem-  
 646 ber). Effect of the mirror force on the collision rate due to energetic electron  
 647 precipitation: Monte Carlo simulations. *Earth, Planets and Space*, *75*(1), 117.  
 648 doi: 10.1186/s40623-023-01871-y
- 649 Kelley, M. C. (2009). *The Earth's ionosphere: Plasma physics and electrodynamics*.  
 650 Academic press.
- 651 Kennel, C. F., & Engelmann, F. (1966, November). Velocity Space Diffusion from  
 652 Weak Plasma Turbulence in a Magnetic Field. *Physics of Fluids*, *9*, 2377-2388.

- 653           doi: 10.1063/1.1761629
- 654 Kennel, C. F., & Petschek, H. E. (1966, January). Limit on Stably Trapped Particle  
655           Fluxes. *J. Geophys. Res.*, *71*, 1-28.
- 656 Keskinen, M. J., & Ossakow, S. L. (1983, January). Nonlinear evolution of convect-  
657           ing plasma enhancements in the auroral ionosphere, 2. Small scale irregulari-  
658           ties. *J. Geophys. Res.*, *88*(A1), 474-482. doi: 10.1029/JA088iA01p00474
- 659 Kintner, P. M., Ledvina, B. M., & de Paula, E. R. (2007, September). GPS  
660           and ionospheric scintillations. *Space Weather*, *5*(9), 09003. doi: 10.1029/  
661           2006SW000260
- 662 Komjathy, A. (1997). *Global ionospheric total electron content mapping using the*  
663           *global positioning system* (Unpublished doctoral dissertation). University of  
664           New Brunswick, Canada.
- 665 Komjathy, A., Sparks, L., Wilson, B. D., & Mannucci, A. J. (2005, December).  
666           Automated daily processing of more than 1000 ground-based GPS receivers  
667           for studying intense ionospheric storms. *Radio Science*, *40*(6), RS6006. doi:  
668           10.1029/2005RS003279
- 669 Komjathy, A., Yang, Y.-M., Meng, X., Verkhoglyadova, O., Mannucci, A. J.,  
670           & Langley, R. B. (2016, July). Review and perspectives: Understand-  
671           ing natural-hazards-generated ionospheric perturbations using GPS mea-  
672           surements and coupled modeling. *Radio Science*, *51*(7), 951-961. doi:  
673           10.1002/2015RS005910
- 674 Le Contel, O., Roux, A., Robert, P., Coillot, C., Bouabdellah, A., de La Porte,  
675           B., ... Larson, D. (2008, December). First Results of the THEMIS  
676           Search Coil Magnetometers. *Space Sci. Rev.*, *141*, 509-534. doi: 10.1007/  
677           s11214-008-9371-y
- 678 Lessard, M. R., & Knudsen, D. J. (2001, October). Ionospheric reflection of small-  
679           scale Alfvén waves. *Geophys. Res. Lett.*, *28*(18), 3573-3576. doi: 10.1029/  
680           2000GL012529
- 681 Li, L., Omura, Y., Zhou, X.-Z., Zong, Q.-G., Rankin, R., Yue, C., & Fu, S.-  
682           Y. (2022, May). Nonlinear Wave Growth Analysis of Chorus Emissions  
683           Modulated by ULF Waves. *Geophys. Res. Lett.*, *49*(10), e97978. doi:  
684           10.1029/2022GL097978
- 685 Li, L., Omura, Y., Zhou, X.-Z., Zong, Q.-G., Rankin, R., Yue, C., ... Ren, J. (2023,

- 686 February). Chorus Wave Generation Modulated by Field Line Resonance and  
 687 Mirror-Mode ULF Waves. *Journal of Geophysical Research (Space Physics)*,  
 688 *128*(2), e2022JA031127. doi: 10.1029/2022JA031127
- 689 Li, W., Bortnik, J., Thorne, R. M., & Angelopoulos, V. (2011, December). Global  
 690 distribution of wave amplitudes and wave normal angles of chorus waves  
 691 using THEMIS wave observations. *J. Geophys. Res.*, *116*, 12205. doi:  
 692 10.1029/2011JA017035
- 693 Li, W., Bortnik, J., Thorne, R. M., Nishimura, Y., Angelopoulos, V., & Chen, L.  
 694 (2011, June). Modulation of whistler mode chorus waves: 2. Role of density  
 695 variations. *J. Geophys. Res.*, *116*, A06206. doi: 10.1029/2010JA016313
- 696 Li, W., Thorne, R. M., Bortnik, J., Nishimura, Y., & Angelopoulos, V. (2011, June).  
 697 Modulation of whistler mode chorus waves: 1. Role of compressional Pc4-5  
 698 pulsations. *J. Geophys. Res.*, *116*, A06205. doi: 10.1029/2010JA016312
- 699 Lyons, L. R. (1974, December). Pitch angle and energy diffusion coefficients from  
 700 resonant interactions with ion-cyclotron and whistler waves. *Journal of Plasma  
 701 Physics*, *12*, 417-432. doi: 10.1017/S002237780002537X
- 702 Lysak, R. L. (1991, February). Feedback instability of the ionospheric resonant cav-  
 703 ity. *J. Geophys. Res.*, *96*(A2), 1553-1568. doi: 10.1029/90JA02154
- 704 Ma, Q., Connor, H. K., Zhang, X. J., Li, W., Shen, X. C., Gillespie, D., ... Spence,  
 705 H. E. (2020, August). Global Survey of Plasma Sheet Electron Precipitation  
 706 due to Whistler Mode Chorus Waves in Earth's Magnetosphere. *Geophys.  
 707 Res. Lett.*, *47*(15), e88798. doi: 10.1029/2020GL088798
- 708 Makarevich, R. A., Crowley, G., Azeem, I., Ngwira, C., & Forsythe, V. V. (2021,  
 709 May). Auroral E Region as a Source Region for Ionospheric Scintillation.  
 710 *Journal of Geophysical Research (Space Physics)*, *126*(5), e29212. doi:  
 711 10.1029/2021JA029212
- 712 Mannucci, A. J., Wilson, B. D., Yuan, D. N., Ho, C. H., Lindqwister, U. J., &  
 713 Runge, T. F. (1998, May). A global mapping technique for GPS-derived  
 714 ionospheric total electron content measurements. *Radio Science*, *33*(3), 565-  
 715 582. doi: 10.1029/97RS02707
- 716 McCaffrey, A. M., & Jayachandran, P. T. (2017, June). Observation of subsecond  
 717 variations in auroral region total electron content using 100 Hz sampling of  
 718 GPS observables. *Journal of Geophysical Research (Space Physics)*, *122*(6),

- 719 6892-6900. doi: 10.1002/2017JA024255
- 720 McCaffrey, A. M., & Jayachandran, P. T. (2019, February). Determination of the  
721 Refractive Contribution to GPS Phase “Scintillation”. *Journal of Geophysical*  
722 *Research (Space Physics)*, *124*(2), 1454-1469. doi: 10.1029/2018JA025759
- 723 McFadden, J. P., Carlson, C. W., Larson, D., Ludlam, M., Abiad, R., Elliott, B.,  
724 ... Angelopoulos, V. (2008, December). The THEMIS ESA Plasma In-  
725 strument and In-flight Calibration. *Space Sci. Rev.*, *141*, 277-302. doi:  
726 10.1007/s11214-008-9440-2
- 727 McPherron, R. L. (1972, September). Substorm related changes in the geomagnetic  
728 tail: The growth phase. *Planetary Space Science*, *20*, 1521-1539. doi: 10.1016/  
729 0032-0633(72)90054-2
- 730 Meng, X., Mannucci, A. J., Verkhoglyadova, O. P., & Tsurutani, B. T. (2016, April).  
731 On forecasting ionospheric total electron content responses to high-speed solar  
732 wind streams. *Journal of Space Weather and Space Climate*, *6*, A19. doi:  
733 10.1051/swsc/2016014
- 734 Meng, X., Mannucci, A. J., Verkhoglyadova, O. P., Tsurutani, B. T., Ridley, A. J.,  
735 & Shim, J.-S. (2020, February). Thermosphere-Ionosphere Modeling With  
736 Forecastable Inputs: Case Study of the June 2012 High-Speed Stream Geo-  
737 magnetic Storm. *Space Weather*, *18*(2), e02352. doi: 10.1029/2019SW002352
- 738 Meng, X., Ozturk, D. S., Verkhoglyadova, O. P., Varney, R. H., Reimer, A. S., Seme-  
739 ter, J. L., ... Zhan, W. (2022, December). Energy Deposition by Mesoscale  
740 High-Latitude Electric Fields Into the Thermosphere During the 26 October  
741 2019 Geomagnetic Storm. *Journal of Geophysical Research (Space Physics)*,  
742 *127*(12), e2022JA030716. doi: 10.1029/2022JA030716
- 743 Meredith, N. P., Bortnik, J., Horne, R. B., Li, W., & Shen, X.-C. (2021). Statisti-  
744 cal investigation of the frequency dependence of the chorus source mechanism  
745 of plasmaspheric hiss. *Geophysical Research Letters*, *48*(6), e2021GL092725.  
746 Retrieved from [https://agupubs.onlinelibrary.wiley.com/doi/abs/](https://agupubs.onlinelibrary.wiley.com/doi/abs/10.1029/2021GL092725)  
747 [10.1029/2021GL092725](https://doi.org/10.1029/2021GL092725) (e2021GL092725 2021GL092725) doi: [https://](https://doi.org/10.1029/2021GL092725)  
748 [doi.org/10.1029/2021GL092725](https://doi.org/10.1029/2021GL092725)
- 749 Miyoshi, Y., Katoh, Y., Nishiyama, T., Sakanoi, T., Asamura, K., & Hirahara, M.  
750 (2010, October). Time of flight analysis of pulsating aurora electrons, consid-  
751 ering wave-particle interactions with propagating whistler mode waves. *J.*

- 752 *Geophys. Res.*, *115*, A10312. doi: 10.1029/2009JA015127
- 753 Moen, J., Oksavik, K., Alfonsi, L., Daabakk, Y., Romano, V., & Spogli, L. (2013,  
754 January). Space weather challenges of the polar cap ionosphere. *Journal of*  
755 *Space Weather and Space Climate*, *3*, A02. doi: 10.1051/swsc/2013025
- 756 Morton, Y. J., Yang, Z., Breitsch, B., Bourne, H., & Rino, C. (2020). Ionospheric ef-  
757 fects, monitoring, and mitigation techniques. In *Position, navigation, and tim-*  
758 *ing technologies in the 21st century* (p. 879-937). John Wiley Sons, Ltd. doi:  
759 <https://doi.org/10.1002/9781119458449.ch31>
- 760 Newell, P. T., Sotirelis, T., & Wing, S. (2009, September). Diffuse, monoenergetic,  
761 and broadband aurora: The global precipitation budget. *J. Geophys. Res.*,  
762 *114*, A09207. doi: 10.1029/2009JA014326
- 763 Nishimura, Y., Bortnik, J., Li, W., Thorne, R. M., Lyons, L. R., Angelopoulos, V.,  
764 ... Auster, U. (2010, October). Identifying the Driver of Pulsating Aurora.  
765 *Science*, *330*, 81-84. doi: 10.1126/science.1193186
- 766 Nishimura, Y., Bortnik, J., Li, W., Thorne, R. M., Ni, B., Lyons, L. R., ... Auster,  
767 U. (2013, Feb). Structures of dayside whistler-mode waves deduced from  
768 conjugate diffuse aurora. *Journal of Geophysical Research (Space Physics)*,  
769 *118*(2), 664-673. doi: 10.1029/2012JA018242
- 770 Nishimura, Y., Kelly, T., Jayachandran, P. T., Mrak, S., Semeter, J. L., Dono-  
771 van, E. F., ... Nishitani, N. (2023, August). Nightside High-Latitude  
772 Phase and Amplitude Scintillation During a Substorm Using 1-Second Scin-  
773 tillation Indices. *Journal of Geophysical Research (Space Physics)*, *128*(8),  
774 e2023JA031402. doi: 10.1029/2023JA031402
- 775 Nishimura, Y., Mrak, S., Semeter, J. L., Coster, A. J., Jayachandran, P. T., Groves,  
776 K. M., ... Ruohoniemi, J. M. (2021, June). Evolution of Mid-latitude Density  
777 Irregularities and Scintillation in North America During the 7-8 September  
778 2017 Storm. *Journal of Geophysical Research (Space Physics)*, *126*(6), e29192.  
779 doi: 10.1029/2021JA029192
- 780 Okuzawa, T., & Davies, K. (1981, March). Pulsations in total columnar elec-  
781 tron content. *J. Geophys. Res.*, *86*(A3), 1355-1364. doi: 10.1029/  
782 JA086iA03p01355
- 783 Pi, X., Mannucci, A. J., Lindqwister, U. J., & Ho, C. M. (1997, September). Mon-  
784 itoring of global ionospheric irregularities using the Worldwide GPS Network.

- 785 *Geophys. Res. Lett.*, 24(18), 2283-2286. doi: 10.1029/97GL02273
- 786 Picone, J. M., Hedin, A. E., Drob, D. P., & Aikin, A. C. (2002, December).  
 787 NRLMSISE-00 empirical model of the atmosphere: Statistical comparisons and  
 788 scientific issues. *Journal of Geophysical Research (Space Physics)*, 107(A12),  
 789 1468. doi: 10.1029/2002JA009430
- 790 Pilipenko, V., Belakhovsky, V., Murr, D., Fedorov, E., & Engebretson, M. (2014,  
 791 June). Modulation of total electron content by ULF Pc5 waves. *Jour-  
 792 nal of Geophysical Research (Space Physics)*, 119(6), 4358-4369. doi:  
 793 10.1002/2013JA019594
- 794 Prikryl, P., Jayachandran, P. T., Chadwick, R., & Kelly, T. D. (2015, May).  
 795 Climatology of GPS phase scintillation at northern high latitudes for the  
 796 period from 2008 to 2013. *Annales Geophysicae*, 33(5), 531-545. doi:  
 797 10.5194/angeo-33-531-2015
- 798 Pulkkinen, A., Bernabeu, E., Thomson, A., Viljanen, A., Pirjola, R., Boteler, D.,  
 799 ... MacAlester, M. (2017, Jul). Geomagnetically induced currents: Science,  
 800 engineering, and applications readiness. *Space Weather*, 15(7), 828-856. doi:  
 801 10.1002/2016SW001501
- 802 Ridley, A. J., Deng, Y., & Tóth, G. (2006, May). The global ionosphere thermo-  
 803 sphere model. *Journal of Atmospheric and Solar-Terrestrial Physics*, 68(8),  
 804 839-864. doi: 10.1016/j.jastp.2006.01.008
- 805 Rino, C. (2011). *The theory of scintillation with applications in remote sensing*.  
 806 John Wiley & Sons.
- 807 Sandhu, J. K., Rae, I. J., Staples, F. A., Hartley, D. P., Walach, M. T., Elsdén, T.,  
 808 & Murphy, K. R. (2021, July). The Roles of the Magnetopause and Plasma-  
 809 pause in Storm-Time ULF Wave Power Enhancements. *Journal of Geophysical  
 810 Research (Space Physics)*, 126(7), e29337. doi: 10.1029/2021JA029337
- 811 Santolík, O., Gurnett, D. A., Pickett, J. S., Parrot, M., & Cornilleau-Wehrin, N.  
 812 (2003, July). Spatio-temporal structure of storm-time chorus. *J. Geophys.  
 813 Res.*, 108, 1278. doi: 10.1029/2002JA009791
- 814 Schunk, R. W., Scherliess, L., Sojka, J. J., Thompson, D. C., Anderson, D. N.,  
 815 Codrescu, M., ... Howe, B. M. (2004, February). Global Assimilation of  
 816 Ionospheric Measurements (GAIM). *Radio Science*, 39(1), RS1S02. doi:  
 817 10.1029/2002RS002794

- 818 Sheng, C., Deng, Y., Zhang, S.-R., Nishimura, Y., & Lyons, L. R. (2020, Febru-  
 819 ary). Relative Contributions of Ion Convection and Particle Precipitation  
 820 to Exciting Large-Scale Traveling Atmospheric and Ionospheric Distur-  
 821 bances. *Journal of Geophysical Research (Space Physics)*, *125*(2), e27342.  
 822 doi: 10.1029/2019JA027342
- 823 Shi, R., Li, W., Ma, Q., Green, A., Kletzing, C. A., Kurth, W. S., . . . Reeves, G. D.  
 824 (2019, February). Properties of Whistler Mode Waves in Earth's Plasmas-  
 825 sphere and Plumes. *Journal of Geophysical Research (Space Physics)*, *124*(2),  
 826 1035-1051. doi: 10.1029/2018JA026041
- 827 Shi, X., Baker, J. B. H., Ruohoniemi, J. M., Hartinger, M. D., Murphy, K. R., Ro-  
 828 driguez, J. V., . . . Angelopoulos, V. (2018, October). Long-Lasting Poloidal  
 829 ULF Waves Observed by Multiple Satellites and High-Latitude SuperDARN  
 830 Radars. *Journal of Geophysical Research (Space Physics)*, *123*(10), 8422-8438.  
 831 doi: 10.1029/2018JA026003
- 832 Shi, X., Zhang, X.-J., Artemyev, A., Angelopoulos, V., Hartinger, M. D., Tsai,  
 833 E., & Wilkins, C. (2022, December). On the Role of ULF Waves in the  
 834 Spatial and Temporal Periodicity of Energetic Electron Precipitation. *Jour-  
 835 nal of Geophysical Research (Space Physics)*, *127*(12), e2022JA030932. doi:  
 836 10.1029/2022JA030932
- 837 Skone, S. (2009, February). Using GPS TEC measurements to detect geomagnetic  
 838 Pc 3 pulsations. *Radio Science*, *44*(19), RS0A27. doi: 10.1029/2008RS004106
- 839 Southwood, D., & Hughes, W. (1983). Theory of hydromagnetic waves in the mag-  
 840 netosphere. *Space Science Reviews*, *35*(4), 301-366.
- 841 Southwood, D. J., & Kivelson, M. G. (1981, Jul). Charged particle behavior in  
 842 low-frequency geomagnetic pulsations 1. Transverse waves. *J. Geophys. Res.*,  
 843 *86*(A7), 5643-5655. doi: 10.1029/JA086iA07p05643
- 844 Spicher, A., Cameron, T., Grono, E. M., Yakymenko, K. N., Buchert, S. C., Clausen,  
 845 L. B. N., . . . Moen, J. I. (2015, January). Observation of polar cap patches  
 846 and calculation of gradient drift instability growth times: A Swarm case study.  
 847 *Geophys. Res. Lett.*, *42*(2), 201-206. doi: 10.1002/2014GL062590
- 848 Spicher, A., Clausen, L. B. N., Miloch, W. J., Lofstad, V., Jin, Y., & Moen, J. I.  
 849 (2017, March). Interhemispheric study of polar cap patch occurrence based on  
 850 Swarm in situ data. *Journal of Geophysical Research (Space Physics)*, *122*(3),

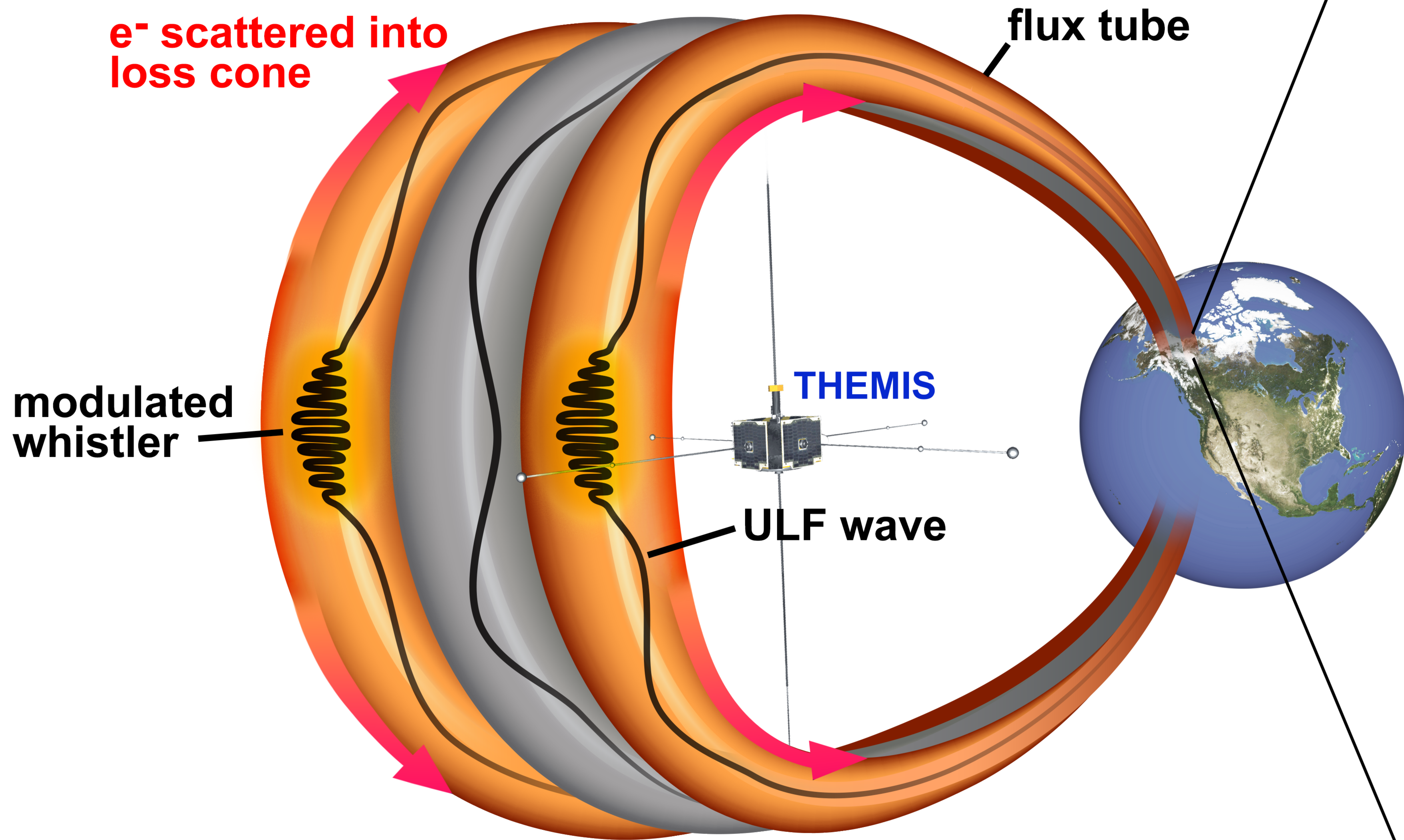


- 851 3837-3851. doi: 10.1002/2016JA023750
- 852 Spogli, L., Alfonsi, L., de Franceschi, G., Romano, V., Aquino, M. H. O., & Dodson,  
853 A. (2009, September). Climatology of GPS ionospheric scintillations over high  
854 and mid-latitude European regions. *Annales Geophysicae*, *27*(9), 3429-3437.  
855 doi: 10.5194/angeo-27-3429-2009
- 856 Streltsov, A. V., & Lotko, W. (2008, May). Coupling between density struc-  
857 tures, electromagnetic waves and ionospheric feedback in the auroral zone.  
858 *Journal of Geophysical Research (Space Physics)*, *113*(A5), A05212. doi:  
859 10.1029/2007JA012594
- 860 Takahashi, K., & Anderson, B. J. (1992, July). Distribution of ULF energy  
861 ( $\leq 80$  mHz) in the inner magnetosphere: A statistical analysis of AMPTE  
862 CCE magnetic field data. *J. Geophys. Res.*, *97*(A7), 10751-10773. doi:  
863 10.1029/92JA00328
- 864 Themens, D. R., Watson, C., Žagar, N., Vasylyevych, S., Elvidge, S., McCaffrey, A.,  
865 ... Jayachandran, P. T. (2022, April). Global Propagation of Ionospheric Dis-  
866 turbances Associated With the 2022 Tonga Volcanic Eruption. *Geophys. Res.*  
867 *Lett.*, *49*(7), e98158. doi: 10.1029/2022GL098158 10.1002/essoar.10510350.1
- 868 Tsurutani, B. T., & Smith, E. J. (1974, January). Postmidnight chorus: A substorm  
869 phenomenon. *J. Geophys. Res.*, *79*, 118-127. doi: 10.1029/JA079i001p00118
- 870 Tsyganenko, N. A. (1995, April). Modeling the Earth's magnetospheric magnetic  
871 field confined within a realistic magnetopause. *J. Geophys. Res.*, *100*, 5599-  
872 5612. doi: 10.1029/94JA03193
- 873 Tyler, E., Breneman, A., Cattell, C., Wygant, J., Thaller, S., & Malaspina, D.  
874 (2019, Mar). Statistical Occurrence and Distribution of High-Amplitude  
875 Whistler Mode Waves in the Outer Radiation Belt. *Geophys. Res. Lett.*,  
876 *46*(5), 2328-2336. doi: 10.1029/2019GL082292
- 877 Verkhoglyadova, O. (2024). *Dataset for the paper "Magnetospheric control of*  
878 *ionospheric TEC perturbations via whistler-mode and ULF waves" paper*  
879 *to be submitted to AGU Advances*. JPL Open Repository. Retrieved from  
880 <https://doi.org/10.48577/jpl.LGI5JS> doi: 10.48577/jpl.LGI5JS
- 881 Verkhoglyadova, O., Meng, X., Mannucci, A. J., Shim, J. S., & McGranaghan,  
882 R. (2020, September). Evaluation of Total Electron Content Prediction  
883 Using Three Ionosphere-Thermosphere Models. *Space Weather*, *18*(9),

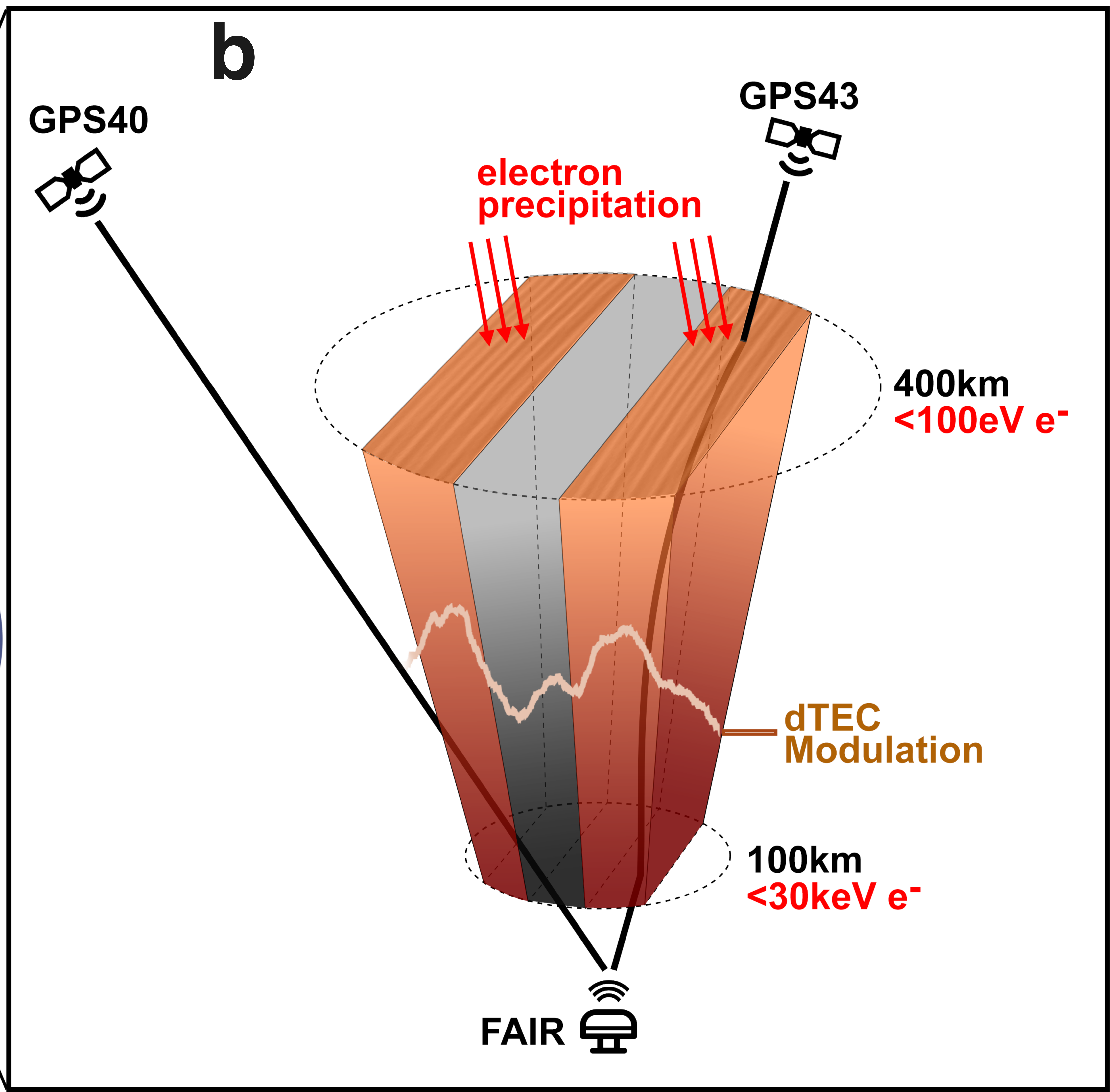
- 884 e2020SW002452. doi: 10.1029/2020SW002452
- 885 Wang, B., Nishimura, Y., Hartinger, M., Sivadas, N., Lyons, L. L., Varney, R. H., &  
886 Angelopoulos, V. (2020, August). Ionospheric Modulation by Storm Time Pc5  
887 ULF Pulsations and the Structure Detected by PFISR-THEMIS Conjunction.  
888 *Geophys. Res. Lett.*, *47*(16), e89060. doi: 10.1029/2020GL089060
- 889 Watson, C., Jayachandran, P. T., & MacDougall, J. W. (2016, May). Characteris-  
890 tics of GPS TEC variations in the polar cap ionosphere. *Journal of Geophysi-  
891 cal Research (Space Physics)*, *121*(5), 4748-4768. doi: 10.1002/2015JA022275
- 892 Watson, C., Jayachandran, P. T., Singer, H. J., Redmon, R. J., & Danskin, D.  
893 (2015, September). Large-amplitude GPS TEC variations associated with  
894 Pc5-6 magnetic field variations observed on the ground and at geosynchronous  
895 orbit. *Journal of Geophysical Research (Space Physics)*, *120*(9), 7798-7821.  
896 doi: 10.1002/2015JA021517
- 897 Watson, C., Jayachandran, P. T., Singer, H. J., Redmon, R. J., & Danskin, D.  
898 (2016, February). GPS TEC response to Pc4 “giant pulsations”. *Jour-  
899 nal of Geophysical Research (Space Physics)*, *121*(2), 1722-1735. doi:  
900 10.1002/2015JA022253
- 901 Watt, C. E. J., Degeling, A. W., Rankin, R., Murphy, K. R., Rae, I. J., & Singer,  
902 H. J. (2011, October). Ultralow-frequency modulation of whistler-mode wave  
903 growth. *Journal of Geophysical Research (Space Physics)*, *116*(A10), A10209.  
904 doi: 10.1029/2011JA016730
- 905 Xia, Z., Chen, L., Dai, L., Claudepierre, S. G., Chan, A. A., Soto-Chavez, A. R.,  
906 & Reeves, G. D. (2016, September). Modulation of chorus intensity by ULF  
907 waves deep in the inner magnetosphere. *Geophys. Res. Lett.*, *43*, 9444-9452.  
908 doi: 10.1002/2016GL070280
- 909 Xia, Z., Chen, L., & Li, W. (2020, November). Statistical Study of Chorus Modula-  
910 tions by Background Magnetic Field and Plasma Density. *Geophys. Res. Lett.*,  
911 *47*(22), e89344. doi: 10.1029/2020GL089344
- 912 Xiong, C., Park, J., Lühr, H., Stolle, C., & Ma, S. Y. (2010, September). Compar-  
913 ing plasma bubble occurrence rates at CHAMP and GRACE altitudes during  
914 high and low solar activity. *Annales Geophysicae*, *28*(9), 1647-1658. doi:  
915 10.5194/angeo-28-1647-2010
- 916 Yeh, K. C., & Liu, C. H. (1982, April). Radio wave scintillations in the ionosphere.

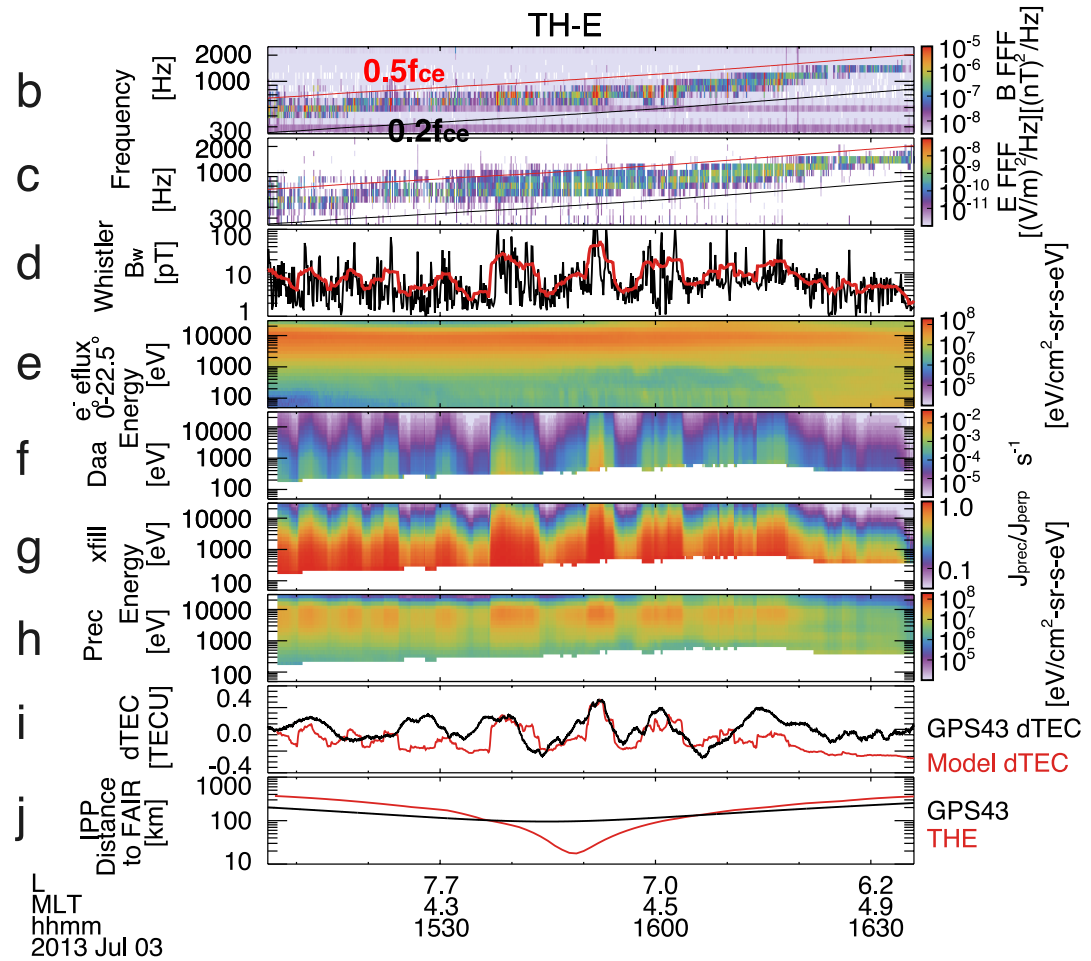
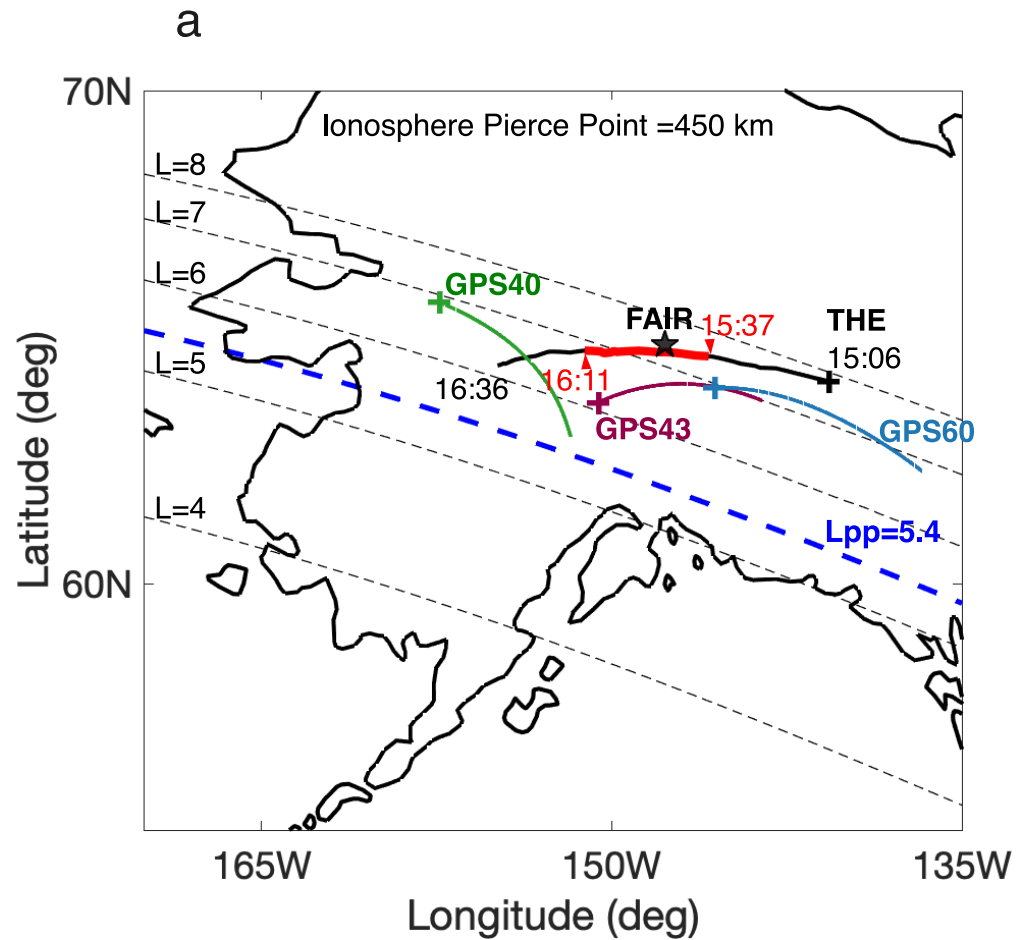
- 917 *IEEE Proceedings*, 70, 324-360.
- 918 Yeoman, T. K., James, M., Mager, P. N., & Klimushkin, D. Y. (2012, June). Super-  
 919 DARN observations of high-m ULF waves with curved phase fronts and their  
 920 interpretation in terms of transverse resonator theory. *Journal of Geophysical  
 921 Research (Space Physics)*, 117(A6), A06231. doi: 10.1029/2012JA017668
- 922 Zettergren, M. D., & Snively, J. B. (2015, September). Ionospheric response  
 923 to infrasonic-acoustic waves generated by natural hazard events. *Jour-  
 924 nal of Geophysical Research (Space Physics)*, 120(9), 8002-8024. doi:  
 925 10.1002/2015JA021116
- 926 Zhai, C., Shi, X., Wang, W., Hartinger, M. D., Yao, Y., Peng, W., ... Baker,  
 927 J. B. H. (2021, July). Characterization of High-m ULF Wave Signa-  
 928 tures in GPS TEC Data. *Geophys. Res. Lett.*, 48(14), e94282. doi:  
 929 10.1029/2021GL094282
- 930 Zhang, S.-R., Vierinen, J., Aa, E., Goncharenko, L. P., Erickson, P. J., Rideout,  
 931 W., ... Spicher, A. (2022, March). 2022 Tonga Volcanic Eruption Induced  
 932 Global Propagation of Ionospheric Disturbances via Lamb Waves. *Frontiers in  
 933 Astronomy and Space Sciences*, 9, 871275. doi: 10.3389/fspas.2022.871275
- 934 Zhang, X. J., Angelopoulos, V., Artemyev, A. V., Hartinger, M. D., & Bortnik, J.  
 935 (2020, October). Modulation of Whistler Waves by Ultra-Low-Frequency Per-  
 936 turbations: The Importance of Magnetopause Location. *Journal of Geophysical  
 937 Research (Space Physics)*, 125(10), e28334. doi: 10.1029/2020JA028334
- 938 Zhang, X.-J., Chen, L., Artemyev, A. V., Angelopoulos, V., & Liu, X. (2019,  
 939 November). Periodic Excitation of Chorus and ECH Waves Modulated by  
 940 Ultralow Frequency Compressions. *Journal of Geophysical Research (Space  
 941 Physics)*, 124(11), 8535-8550. doi: 10.1029/2019JA027201
- 942 Zong, Q., Rankin, R., & Zhou, X. (2017, Dec). The interaction of ultra-low-  
 943 frequency pc3-5 waves with charged particles in Earth's magnetosphere. *Re-  
 944 views of Modern Plasma Physics*, 1(1), 10. doi: 10.1007/s41614-017-0011-4

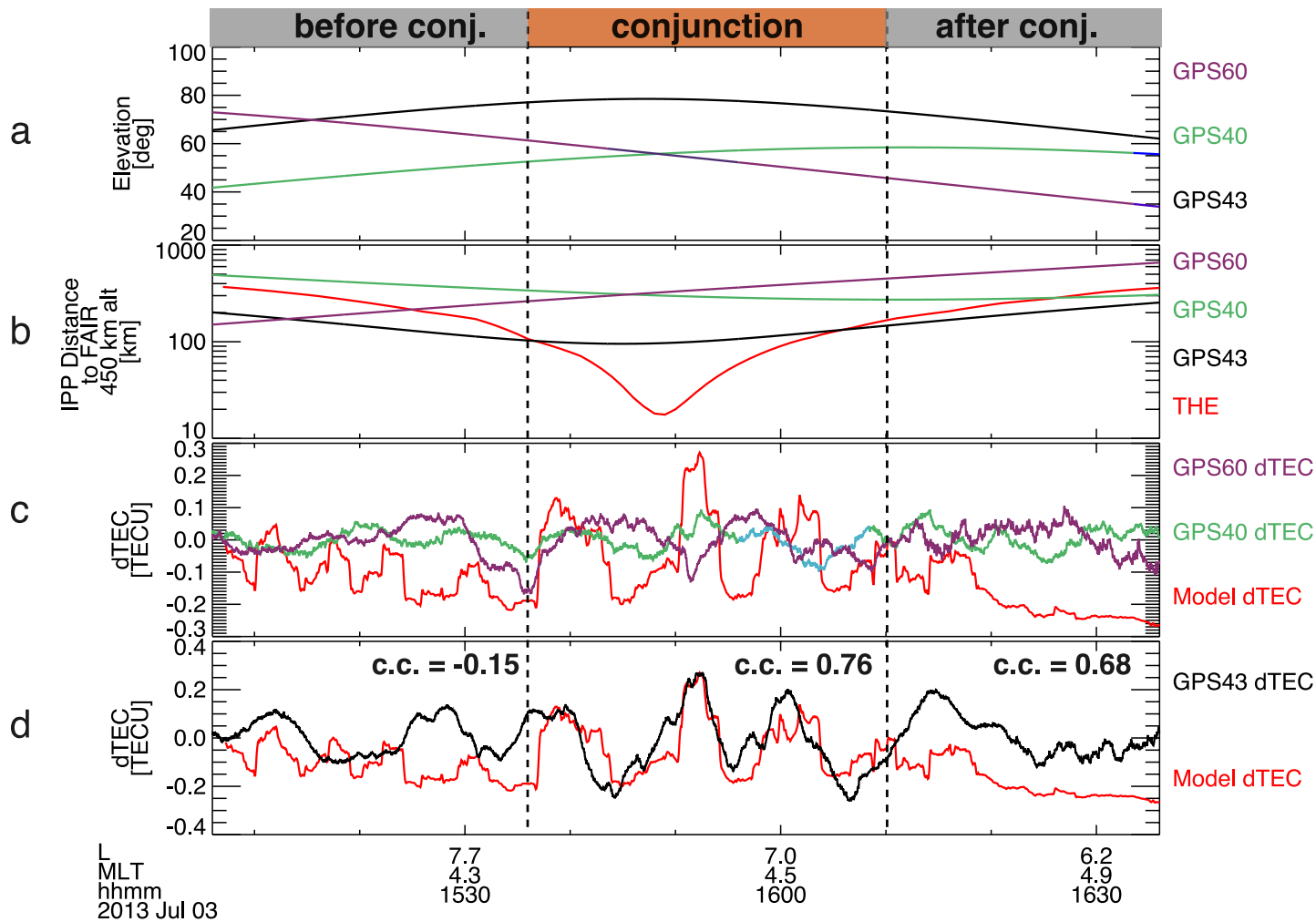
**a**

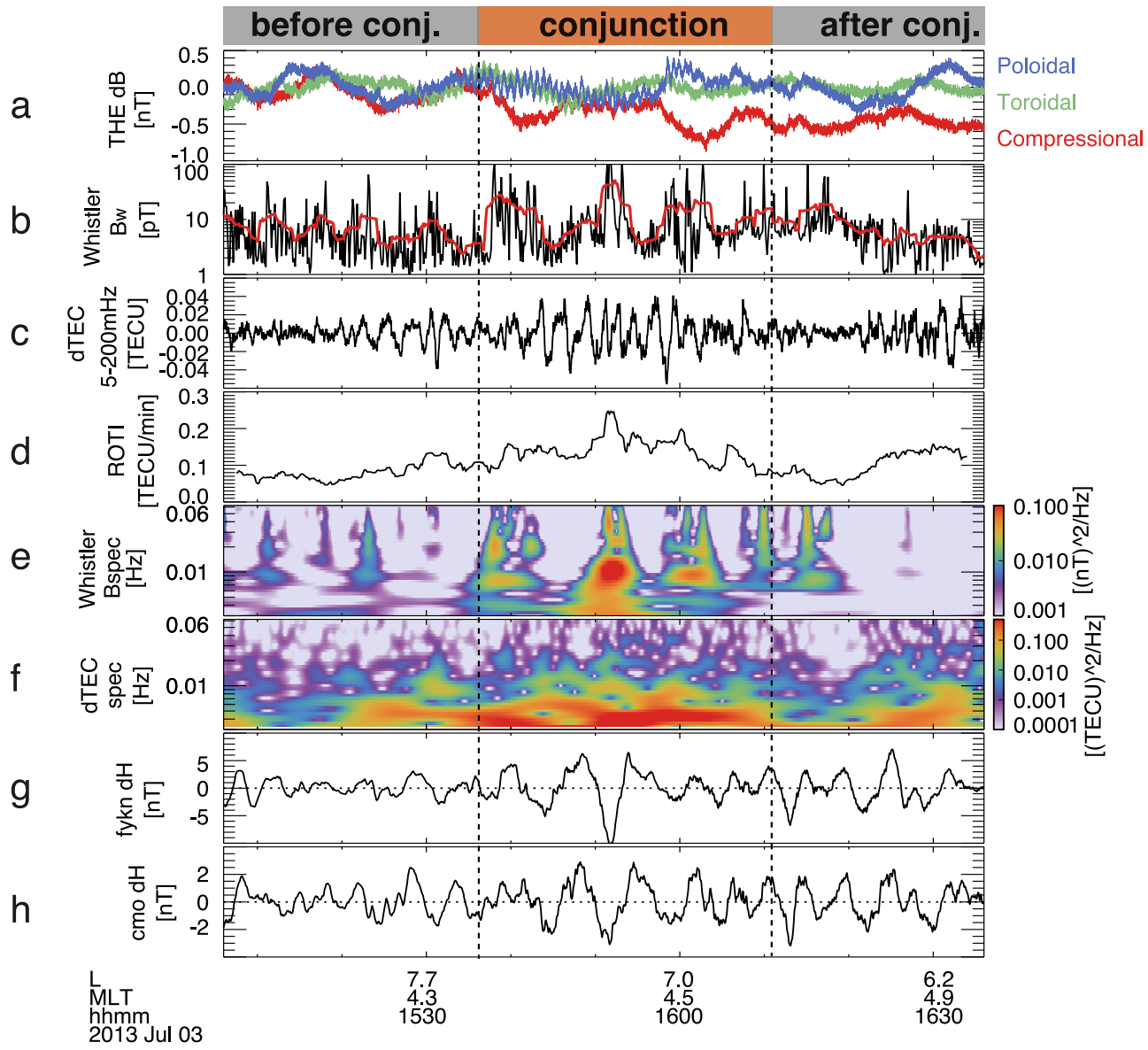


**b**









### Comparison of dTEC and Whistler spectra

